An investigation of the stability of Developing Pipe Flow

Stephen David Williams

A thesis submitted to the University of Manchester

for the degree of Doctor of Philosophy

in the Faculty of Science and Engineering

September 28, 2001

ProQuest LLC.
789 East Eisenhower Parkway
P.O. Box 1346
Ann Arbor, MI 48106 – 1346

Contents

List of Figures

Abstract

This thesis describes the results of an experimental investigation into the finite-amplitude stability of the flow in the entrance of pipes. The research follows on from previous work on the finite stability of fully developed pipe flow, which is thought to be linearly stable. The entrance flow, by contrast, has an instability at Reynolds numbers above approximately 10000.

The flow is disturbed over a finite time by injecting fluid into it. The size of the perturbation determines the probability that the system will undergo sustained transition to turbulence. The probabilities are measured at a range of disturbance amplitudes and the stability is characterised by the amplitude that gives a 0.5 probability of transition. Large numbers of experimental runs are required to calculate this critical amplitude of disturbance with accuracy. Measurements of the sizes of the puffs in the developed flow showed that puff size varies at constant Reynolds number while the speeds of the turbulent-laminar interfaces do not vary.

The first experiments on the developing flow concerned the properties of transition near the lower Reynolds number limit that sustained turbulence is possible, $Re = 2170$. At this Reynolds number the transition to turbulence takes the form of turbulent puffs and the amplitude of disturbance required to bring about transition is comparatively large. It is found that the amplitude of perturbation required changes by a large amount depending upon which part of the flow is disturbed. The form of the finite stability curve was found to be very different from that of the neutral linear stability curve.

These experiments were repeated at Reynolds numbers of three and four thousand. The finite stability curve at these Reynolds numbers showed a greater degree of similarity to the form of the neutral linear stability curve. The investigation ended by examining the average shape of the probability versus amplitude curves.

0.1 Declaration

No portion of the work referred to in this thesis has been submitted in support of an application for another degree or qualification of this or any other university or other institute of learning.

0.2 Acknowledgements

I would like to take this opportunity to especially thank my supervisor, Prof. Tom Mullin, for his patient and expert guidance throughout my PhD.

Many thanks to Graham Tudor for the construction of equipment and the essential maintenance of the pipe apparatus that allowed the experiments to be performed. I am grateful for help of the technicians from the condensed matter group in this respect as well.

I would also like to thank those with whom I had useful discussions including Dr. Anne Juel, Dr. Doug Binks and other members of the Nonlinear Dynamics Group.

Finally I would like to thank Louise Spurgeon for her support and helping to check the text of this document.

This research was funded through a grant from the EPSRC.

Chapter 1

Introduction

1.1 Natural Transition

Fluid flows in pipes fit into two classes, laminar and turbulent. Laminar flow is found at low flow rates in pipes of small diameter. Turbulent flow is the most common type of flow found in industrial and domestic pipe flows. The most important differences between these two types of flow for practical purposes are the increased resistance to motion and increased mixing that occur in turbulent flow.

The transition between these distinct types of flow occurs rapidly without any known intermediate stable states. The flow rate above which the flow becomes turbulent is dependent upon the level of external vibrations and imperfections in the pipe. At low flow rates turbulent flow is not stable and the flow always relaminarises after it has been perturbed. At higher flow rates, where a constant level of disturbance is applied, turbulent patches form intermittently in the laminar flow. These advect down the pipe and remain even after the applied disturbances have been removed. When the flow rate is even higher any disturbances in the pipe cause the flow to rapidly and permanently become turbulent along the entire length of the pipe. However laminar flow can be maintained at high flow rates if external disturbances are controlled and minimised.

Pipe flow belongs to a wider class of shear flows, which do not satisfy the Rayleigh criterion for instability, i.e. their velocity profile does not contain an inflection point. Other examples include plane Poiseuille flow, the pressure-driven flow in a two-dimensional channel and plane Couette flow, the flow between parallel plates which move in opposite directions. In all of these systems laminar flow is always found when the flow rate is low. However at higher flow rates turbulent patches can form as a result of external noise or imperfections in the system. See Dauchot & Daviaud (1995) and references therein for a review of instability in plane Couette flow and Carlson, Widnall & Peters (1982) for that of plane Poiseuille flow.

A distinct class of shear flows include mixing layers and jets which are unstable according to the Rayleigh criterion. In these types of flow the flow rate above which transition occurs is independent of the level of disturbance to the flow and the transition to turbulence is comparatively well understood (Bayly, Orszag & Herbert 1988).

1.2 The Experiments of Reynolds

Reynolds (1883) undertook the first systematic investigation of the transition between laminar and turbulent flow in pipes at Manchester University. It was in this investigation that Reynolds demonstrated that the nature of the flow of water through pipes is a function of just one combination of parameters. This combination is now called the Reynolds number and can be written as

$$Re = \frac{\overline{u}d}{\nu} \tag{1.1}$$

Here the ν is the kinematic viscosity of the fluid, d, the diameter of the pipe, $\overline{u}$ is the mean flow velocity and Re is the Reynolds number. This is the definition of the Reynolds number that is used throughout this thesis.

It is now known that the only parameter in the equations of motion (the Navier-Stokes equations) of a pressure driven flow of a Newtonian fluid is the Reynolds number.

Representing the right hand side of the Navier-Stokes equations by N this statement can be written as

$$\frac{\partial \mathbf{u}}{\partial t} = N(\mathbf{u}, Re)$$

Note that this does not mean that two flows at the same Reynolds number and with the same boundary conditions will be of the same type. For example, in pipe flow, one pipe flow may be laminar and another turbulent, at the same Reynolds number, depending upon the history of the systems.

By disturbing the flow as it entered the pipe, Reynolds discovered that pipe flow becomes turbulent at Reynolds numbers above 2000 . However, it was also found that laminar flow can be maintained at high Reynolds numbers when the level of disturbance is small.

The reason why sustained turbulence is not possible below $Re = 2000$ can be inferred using the following argument. The plot of pressure drop versus Reynolds number for disturbed entrance flow, is shown in figure 1.1. The low Reynolds number relationship is linear while at higher Reynolds numbers the flow becomes turbulent and the drag follows a power law. At intermediate Reynolds numbers turbulent patches form intermittently in the laminar flow. The value of the resistance then depends upon the proportion of the flow taken up by turbulent patches.

The turbulent and laminar drag relationships predict the same value for the drag at $Re \approx 1100$. Below 1100 the trend would predict that the resistance to motion of the turbulent flow would be less than that for laminar flow. This situation is non-physical and implies that there are no stable turbulent states at Reynolds numbers below 1100. However it is not clear why the flow cannot become turbulent immediately above $Re = 1100$ but only when the Reynolds number reaches 2000.

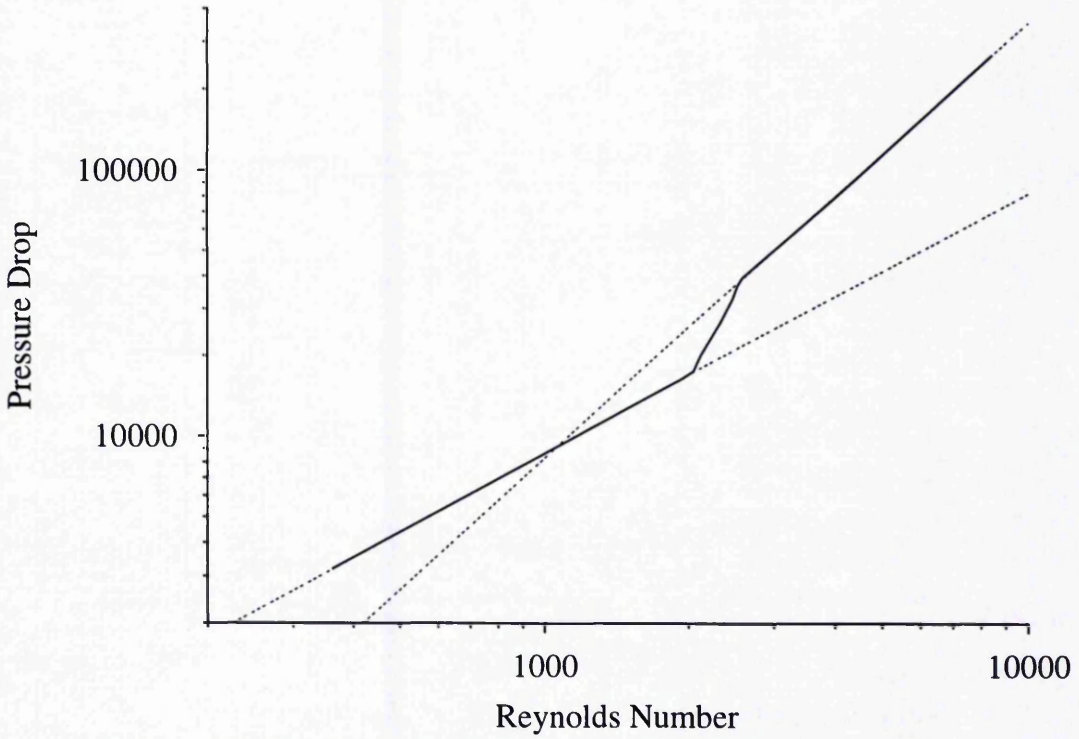

FIGURE 1.1. A plot of the pressure gradient against Reynolds number for pipe flow in the presence of disturbances using the data in Reynolds (1883). The pressure gradient has been non-dimensionalised by dividing it by the pressure gradient at Reynolds number equals one. This non-dimensionalisation makes the relationship valid for all flows of Newtonian fluids through long pipes regardless of the diameter of the pipe and the viscosity of the fluid. The dotted lines are the theoretical resistance laws for pipe flow and the solid lines are fits to Reynolds experimental data.

1.3 Laminar Flow

The laminar flow of a Newtonian fluid through a long cylindrical pipe is an exact solution of the equations of fluid motion. The flow profile is best represented in cylindrical polar coordinates (r, θ, x). The velocity depends only upon the radial coordinate and the flow profile has a parabolic shape given by this equation,

$$\mathbf{u}(r) = 2\overline{u}\left(1 - 4\left[\frac{r}{d}\right]^2\right)\hat{\mathbf{x}} \tag{1.2}$$

The flow velocity is zero at the walls increasing to twice the mean flow velocity in the centre of the pipe. This flow is known as Hagen-Poiseuille flow and is found in practise toward the end of long pipes. Near to the inlet however the flow profile will change with distance along the pipe. Viscous effects diffuse from the walls the flow develops toward a parabolic form.

Since the late nineteenth century numerous researchers have calculated the flow in the entrance of pipes using a variety of methods. Here the principles behind three classes of methods are outlined.

One method involves approximating the Navier-Stokes with a linear equation that can be solved more easily. This was the approach used by Sparrow, Lin & Lundgren (1964). The linearised equations can be solved numerically to give an equation for the flow profile at different downstream locations.

The developing flow profile has also been simulated on computer using direct numerical simulation (Hornbeck 1963). Direct numerical simulation is discussed in more detail later in this chapter. These methods do not require the linearisation of the equations of motion and are, therefore, more reliable than the previous method (Fargie & Martin 1971, Gupta & Garg 1981). The result of these simulations is a table of flow velocities at different locations in the pipe. For many purposes this is not as useful as the continuous analytic functions for the flow profiles that are obtained with the previous method.

It is possible to use the shape of the developing flow profile found using the above methods to reduce the equations to a more easily solvable form. The known form of the flow profile is used to integrate the equations of motion into a set of ordinary differential equations. This integral form of the equations of motion can be solved using standard numerical methods such as Runge-Kutta. Examples of the use of this method can be found in Mohanty & Asthana (1978) and Fargie & Martin (1971).

The flow profile of developing flow has been measured by several researchers (see Fargie & Martin 1971) . The level of agreement between the different measurements is similar to that between the different theoretical predictions.

A 3-dimensional plot of streamwise velocity with distance from the centre of the pipe and distance down the tube is shown in figure 1.2. The data is taken from the paper by Mohanty & Asthana (1978) and illustrates the main properties of the developing flow. The flow profile near the inlet is flat in the centre of the pipe. The velocity of this central core of fluid increases as the region shrinks in size downstream. The shape of flow profile depends only upon the quotient of the distance from the inlet, measured in pipe diameters, and the Reynolds number.

Further it is found that the fully developed Hagen-Poiseuille is only reached in the limit of large downstream distance from the inlet. Because of this all experiments in so-called fully established pipe flow are performed on flows where the fluid velocities are all within $95\ \% - 99\ \%$ of the fully developed value.

1.4 Theoretical Analysis of Fully Developed Pipe Flow

The observation that laminar flow can be maintained at high Reynolds number has been supported by linear stability theory. Linear stability concerns the evolution of infinitesimal perturbations, for which the equations of motion are reduced to an eigenvalue equation. The eigenvalues are complex and the real and imaginary parts give the propagation

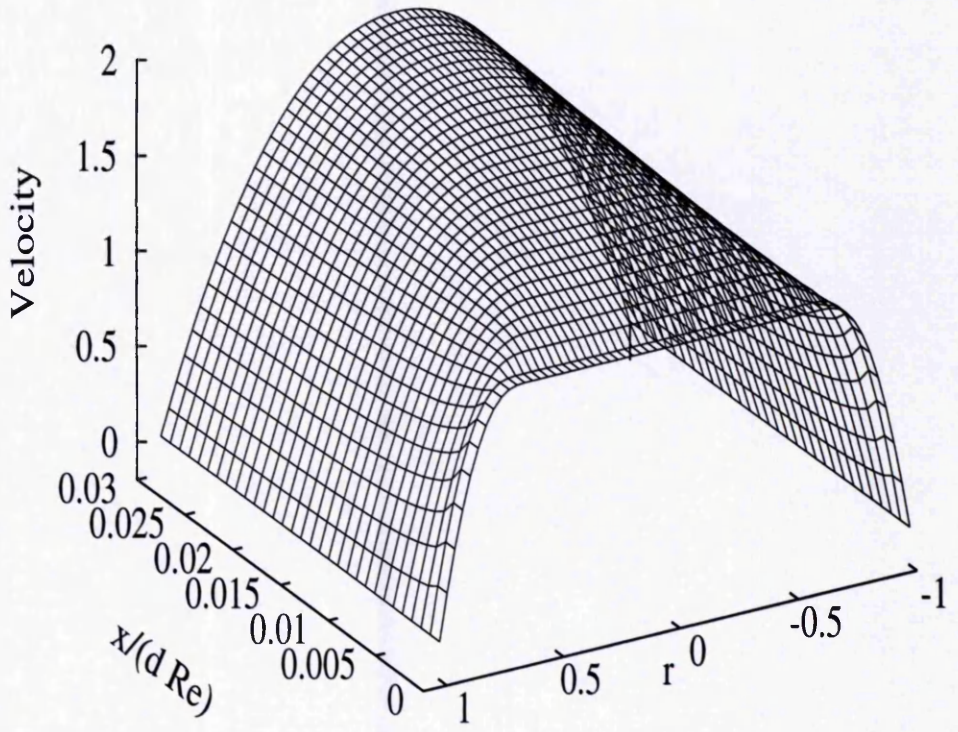

FIGURE 1.2. The flow profile at different distances downstream of the inlet at $Re = 2170$. All of the units are non-dimensionalised, the distance from the inlet is in pipe diameters, the distance from the centre of the tube is in pipe radii and the velocity is in multiples of the mean velocity.

speed and growth rate of the corresponding eigenfunction (mode). The eigenvalue equation for Hagen-Poiseuille flow has not been solved for all possible forms of infinitesimal disturbance. The calculation of the growth rates of axisymmetric modes has not revealed any growing modes (see Drazin & Reid (1981) and references therein). Together with analogies from the equations of linear stability for plane Couette flow, where linear stability has been proved (Romanov 1973), it seems likely that Hagen-Poiseuille flow is stable to infinitesimal axisymmetric perturbations. The evolution of non-axisymmetric modes has been investigated using numerical simulation by workers including Salwen & Grosch (1972). The results suggest that Poiseuille flow is stable to all infinitesimal perturbations.

The experiments of Leite (1959) confirmed some of the linear stability calculations from measurements of the flow patterns that evolve from small disturbances to the flow. Pfenninger (1961) maintained laminar flow in a cylindrical wind tunnel at Reynolds numbers in excess of 10^6 confirming that pipe flow is stable at high Reynolds numbers.

Plane Poiseuille flow differs from both Hagen-Poiseuille and Couette flow as it has a linearly unstable mode at $Re = 5772$. However, plane Poiseuille can only be maintained at that high Reynolds number when the level of external vibrations or imperfections in the system are low. Under less controlled conditions transition is found to occur at Reynolds numbers between 1000 and 2000 (Nishioka, Iida & Ichikawa 1975). At these Reynolds numbers the transition to turbulence is found to have a similar form to that in the other two flows.

The lack of any growing modes in pipe Poiseuille flow means that any other stable solutions to fluid flow in a pipe must be disconnected from the Poiseuille flow solution. Hence the transition to turbulence in fully developed pipe flow is perhaps best understood in terms of finite perturbations.

Another stability analysis (which is also linear) is the calculation of the Reynolds number below which all possible flow patterns in a pipe immediately evolve toward Poiseuille flow. The analysis involves calculating the rate of change of the kinetic en-

ergy of the flow that constitutes the difference between the flow pattern in question and Poiseuille flow. The lowest Reynolds number at which this rate of change of energy is non-negative, for all possible flow patterns, was calculated by Joseph & Carmi (1968). They found this critical Reynolds number to be 83. At Reynolds numbers below this value the long time behaviour of Newtonian fluid flow in a pipe is guaranteed to be Poiseuille flow. The theory gives no indication, however, of the evolution of flows at Reynolds numbers in excess of 83.

There has been a great deal of research directed toward the stability of Poiseuille flow to small but finite disturbances. In weakly nonlinear theory the rate of change of the amplitude of a mode is expressed as an expansion in powers of its amplitude. The first term of this expansion is of first order in the amplitude and is simply related to the eigenvalue of the mode in the linear stability calculations. The higher order coefficients are called the Landau constants. As linear stability predicts that the growth rates of all modes are negative in Poiseuille flow the first term in the expansion is negative. Hence for growth the sum of the nonlinear terms in the expansion must be positive. Also the amplitude of the mode must be great enough for the positive contributing higher order terms to dominate over the first linear stability term.

Davey & Nguygen (1971) calculated the first Landau constant for a number of modes. This allowed them to estimate the amplitude of the modes for which there was zero growth (neutral stability). However, examining this mode using numerical simulation Patera & Orszag (1981) found that it decayed. It was suggested that the reason for this disagreement is that the calculation of many Landau constants are required to find equilibrium amplitudes. Sen & Maji (1985) calculated the first 14 Landau coefficients and so were able to assess the state of convergence. They found that for some groups of modes and for some Reynolds numbers the equilibrium amplitudes were inside the radius of convergence, hence, implying neutral stability.

More recently Trefethen, Trefethen, Reddy & Discoll (1993) initiated a large body of work on the role of transient growth in the instability of pipe flow. The basic idea behind

this may be outlined as follows. The eigenfunctions used in the linear stability analysis of Poiseuille flow are non-normal. This means that the energy of a flow pattern is not equal to the sum of the energies of the series of eigenfunctions that make up that flow. Because of this, the energy of flow features can increase in time, despite the fact that all of the amplitudes in the series are reducing, due to linear stability. According to linear stability all of the amplitudes of all of the modes will decay to zero and Poiseuille flow will be regained. This is the reason for the name transient growth.

Transient growth has been observed in the experiments of Keskel (1961) at a Reynolds number of 7600. Subsequent analysis of these results showed them to be consistent with transient growth theory as discussed by Mayor & Reskotko (1997).

The energy amplification due to transient growth is already large at $Re = 2000$ and increases with Reynolds number. The large energy amplifications could act as a bridge across the region of linear stability that lies between Poiseuille flow and stable turbulent states. Hence work has been carried out to find the optimally amplified mode. Bergstrom (1993) found that the modes with the greatest growth rates had an azimuthal wave number of one. Following on from this Schmid (1994) searched for the mode with the greatest amplification at Reynolds number 3000. Those flow patterns were investigated because the modes with the lowest decay rates in linear stability theory have an azimuthal wave number of one. They found that the optimally amplified mode has a flow profile which is independent of location down the tube.

There has been further work on the evolution of this mode using linear stability analysis (Zikanov 1996). When the mode reaches sufficient amplitude a point of inflection is created in the flow profile. It was found that following the formation of the point of inflection the flow becomes linearly unstable. The growth of new modes due to the linear instability can exceed the rate of decay of the transiently amplified mode. Further interactions that act upon these newly created modes may sustain the growth of the perturbation until the flow resembles that of turbulence.

The importance of transiently amplified modes in the transition to turbulence is not

yet clear, however. This is illustrated in the paper by Dauchot & Manneville (1997). They take a simple system, for which the general dynamics can be calculated, and compare the true evolution with the predictions of transient growth. In this system it is found that transient growth predicts the dynamics only near the trivial state, the full nonlinear evolution bears no resemblance to the transient growth results.

Another approach to finding the evolution of transiently amplified modes in the nonlinear regime has been to investigate the interactions between the modes due to nonlinearity. Without nonlinear effects the transiently amplified flow features will inevitably decay. The nonlinear term in the Navier-Stokes equations effectively introduces an interaction between modes and allows the excitation of new ones. If these new modes are transiently amplified a feedback loop occurs.

There are selection rules that govern which modes can interact with one another as discussed by Boberg & Brosa (1988). Another requirement for transient growth is that the flow must contain modes that are far from orthogonal and this means that of the order of one hundred modes may be required for feedback (Grossmann 2000). This is in contrast to systems that have a linear instability and which, near the first instability, can be understood by considering just one mode.

Using general arguments about the nature of the transiently amplified modes and that of nonlinear interactions, it is possible to make predictions about the amplitude of perturbation required for amplification. In particular it is possible to calculate how the critical amplitude for amplification scales with Reynolds number. The amplitude, A_c, is predicted to vary as,

$$A_c \propto Re^{-\gamma} \tag{1.3}$$

Considering only transient growth and assuming that transition occurs whenever a perturbation exceeds some amplitude the analysis of Reddy & Henningson (1993) would predict $\gamma = 2$. Analysing the requirements for a feedback loop to be sustained gives $\gamma = 1$ as shown discussed in Grossmann (2000). The model proposed by Bergstrom

(1993) again concerned the evolution of modes in the nonlinear regime but restricts itself to the small number of modes that are least damped by linear stability. This analysis results in a value of γ of 3.

It is important to point out that none of this analysis can explain the main experimental observation in pipe flow transition, that turbulence can only be sustained at Reynolds numbers above 2000. The factor that is missing from all of the theories is knowledge of the turbulent states that the flow evolves into after it has been perturbed.

1.5 Numerical Simulations of Pipe Flow

The evolution of finite perturbations applied to fully developed pipe flow has been calculated using numerical simulation. In order to simulate the Navier-stokes equations on a computer the continuous time and space domains must be discretised. The space domain, can be split into a three-dimensional grid or the flow features can be decomposed into modes. In both cases the evolution of the flow is calculated using finite time steps. The first method of discretisation is the most intuitive and is known as direct numerical simulation (DNS). In the second method there is a choice as to which modes to use. Solutions of the steady linearised Navier-stokes equations, Fourier modes and polynomials have all been used. The right choice of modes can substantially decrease the amount of computing time required for a similar quality of results.

It is only possible to study a finite length of pipe flow to get results in finite time. The ends of this flow domain are either joined or forced to have the Poiseuille flow profile. In either case the numerical simulation will fail to model flow features that approach the length of the flow domain.

A recent example of the use of DNS is given in the work of Eggels *et al.* (1994) who simulated turbulent pipe flow at $Re = 5300$. The simulation took place in a domain five pipe diameters in length. This length was split into 256 equal sections, each section was

subdivided into 128 equally sized sectors. These sectors were split in the radial direction 95 times, with an increased resolution of the grid near the walls. Each calculation advanced the simulation 3×10^{-3} non-dimensional time periods. Here one time period is the time taken for an element of the flow moving at the mean flow velocity to cover one pipe diameter. The simulations used 160 hours of CPU time on a Cray computer to complete 207 non-dimensional time periods. They compared these results to an experiment (also reported in Eggels *et al.* (1994)) performed at the same parameters. There is good agreement in the mean flow profile, the wave number spectrum and statistical correlations in the turbulent flow.

Shan, Zhang & Nieuwstadt (1998) used DNS to calculate the evolution of disturbances caused by fluid being added and removed from the flow. The effects were found to depend upon the distribution of injected fluid as well as its velocity. When the fluid velocity (disturbance amplitude) was too small the disturbance was not amplified. Higher disturbance amplitudes caused the flow to evolve into a complex time dependent state. This behaviour is consistent with what is found in experiments on pipe flow. However they did not find the change in stability that is found experimentally at Reynolds number 2000.

These simulations could be useful for calculating quantities that cannot be directly measured in experiments. However, they do not in themselves explain the mechanisms behind sustained turbulence.

Boberg & Brosa (1988) performed numerical simulations of turbulent pipe flow which was decomposed into a series of Stokes' modes. During the simulation the interaction between different modes was calculated and gave rise to their theory of "mother" and "daughter" modes in pipe flow. Mothers are modes that grow transiently drawing energy from the main flow. They then transfer some of their energy to other, daughter, modes through nonlinear interactions. Further nonlinear interactions spread the energy over a wide spectrum of modes, some of which are mothers. The cycle sets itself up so that the mothers retain only a small fraction of the total energy. Most of the energy is

contained and dissipated, in the large number of daughters.

These observations were tested in an experiment performed by Pysik & Heber (1992) using magnetic fields to generate the flow patterns in the water. Unfortunately as the magnets had a weak effect upon the flow the experiment had to be carried out in a pipe without any mean flow. This meant that the interactions between the modes and Poiseuille flow could not be measured. However, in this model Poiseuille flow is just a single mode and the interactions between all of the other modes were present. They experimented upon two daughter modes and found that their decay rates were in agreement with theory provided the amplitude of the modes were not too large.

The ideas of mother and daughter modes were published in a paper entitled *Onset of turbulence in a pipe* by Boberg & Brosa (1988). However, it is not clear whether the ideas are more applicable to the transition to turbulence or the understanding turbulence itself.

In all of the above numerical simulations the entire flow domain was in turbulent motion. In experiments turbulent patches are found that propagate in the laminar flow. These were considered in the paper Shan, Ma, Zhang & Nieuwstadt (1998) who carried out simulations in which the flow was initially Poiseuille flow with a block of turbulence in the middle of the domain. In contrast to experiments on pipe flow these regions of turbulence were always found to grow and would eventually fill the numerical flow domain.

1.6 Experimental Studies of Turbulent Puffs and Slugs

Since the time of Reynolds, more advanced experimental techniques have been used to analyse the transition to turbulence. The turbulent patches that Reynolds had observed forming intermittently in the flow were found to have shape and structure. Their properties depend only upon the Reynolds number of the pipe flow (Wygnanski & Champagne 1973).

Wygnanski & Champagne (1973) conducted an extensive investigation of turbulent patches. They classified them into slugs, stable for $Re > 3200$ and puffs stable in the range $2000 < Re < 2700$. Patches at intermediate Reynolds numbers were not classified in their paper; however, it is observed that the properties of turbulent patches change continuously with Reynolds number (Darbyshire & Mullin 1995). In the second part of their investigation Wygnanski *et al.* (1974) investigated puffs formed at Reynolds number 2200. At this Reynolds number puffs do not grow or decay but propagate with constant size and speed. For this reason they are called equilibrium puffs.

Slugs consist of an area of turbulence bounded upstream and downstream by distinct turbulent-laminar interfaces. These two interfaces have an identical parabolic shape which remains unaltered as the slug propagates. A graph of the centre-line velocity of fluid in pipe flow during the passage of a slug is shown in figure 1.3. The transition from laminar flow outside the slug to turbulent flow in the interior is quite sudden. Turbulent flow inside slugs away from either interface is similar to the turbulent flow found in pipes that have a uniform turbulent intensity along their length. It was noted by Wygnanski & Champagne (1973) that the speed and shape of the interfaces is such that laminar flow enters the slug but fluid in turbulent motion does not leave. There is strong turbulent production at both interfaces caused by the deceleration and shear imposed on laminar fluid entering the slug. It is this combination of turbulent production at the interfaces and the confinement of fluid that is in turbulent motion which causes slugs to have such well-defined interfaces.

Puffs contain fluid with lower turbulent intensities and have more pronounced coherent flow structures. The structure of puffs is outlined in Wygnanski & Friedman (1975) and Bandyopadhyay (1986). Their upstream laminar-turbulent interface is similar in form to the interfaces found in slugs except that it is diffuse near the wall. At their downstream end puffs do not have a sharp laminar-turbulent interface, instead the turbulent intensity reduces to zero over many pipe diameters. The difference between the two laminar-turbulent interfaces in puffs can be seen clearly from the plot of the streamwise

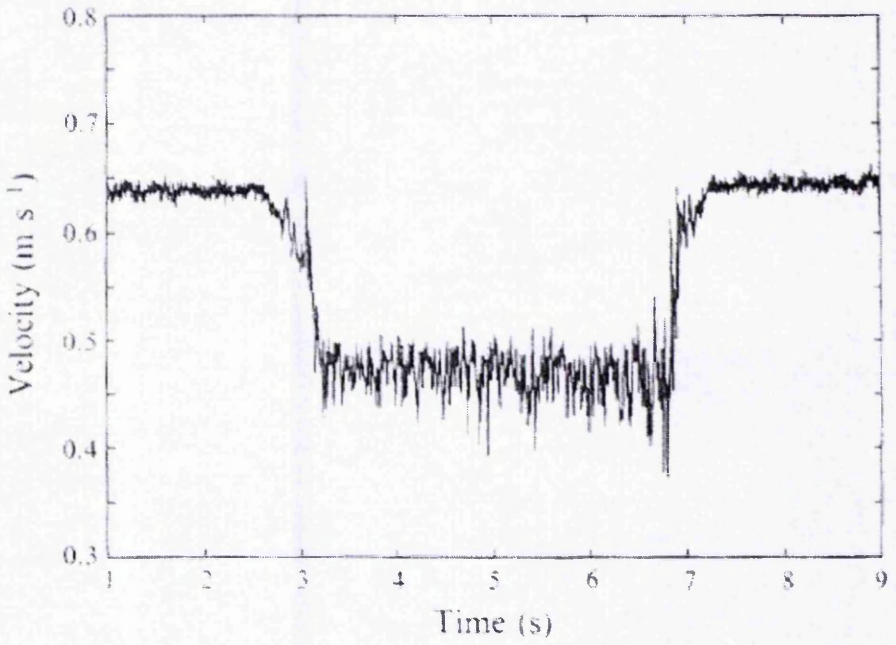

FIGURE 1.3. The component of fluid velocity along the pipe axis in the centre of the pipe during passage of a slug. The fluid velocity was measured using Laser Doppler Velocimetry (LDV). The centre-line velocity reduces as a slug passes because the turbulent flow profile is less pointed than the parabolic laminar flow profile. Hence it can be seen from the diagram that the turbulent intensity increases rapidly along the pipe axis from zero outside the slug to a constant value inside. From Darbyshire & Mullin (1995).

centre-line velocity shown in figure 1.4. This flow patterns inside turbulent puffs are explained in some detail in Bandyopadhyay (1986). To summarise, the difference in the turbulent and laminar flow profiles causes laminar flow to enter the back of the puff, decelerate and mix with turbulent flow. This deceleration and disturbance of the flow leads to intense turbulent production near the upstream interface. This turbulence increases the momentum diffusion, flattening the flow profile causing more deceleration and mixing. In this way puffs are self-sustaining. The diffuse nature of the laminar-turbulent interfaces near the wall is due to the fluid in turbulent motion leaving the puff. The rear interface maintains its shape across the entire cross section and so moves more quickly than some of the fluid near the wall. The slower moving fluid leaves the puff and mixes with the laminar flow upstream of the puff. This fluid slowly relaminarises creating a diffuse laminar-turbulent interface. A similar process of relaminarising and mixing with turbulent flow occurs at the downstream end of the puff causing the gradual change from turbulent to laminar flow that occurs there.

It had been suggested (for example Tritton 1988) that turbulent patches form in pipe flow because of the pressure-fluctuations that occur when the flow becomes turbulent. Turbulent flow increases the drag of the flow and so will reduce the Reynolds number in a pipe flow with a constant pressure head. It is this reduction in the Reynolds number that was thought to cause the relaminarisation of flow behind puffs and slugs. This idea was later disproved, however, in the experiments of Darbyshire & Mullin (1995) who used a piston to draw fluid through a pipe at constant volume flux. Puffs and slugs were found in the flow with similar properties to those in pressure driven systems.

1.7 Stability of Hagen-Poiseuille and plane Couette flow

Investigations into the stability of Poiseuille flow can be grouped into two classes. Those that perturb the flow continuously and those that apply a disturbance over a finite time. Examples of experiments that use each of these two methods will now be outlined.

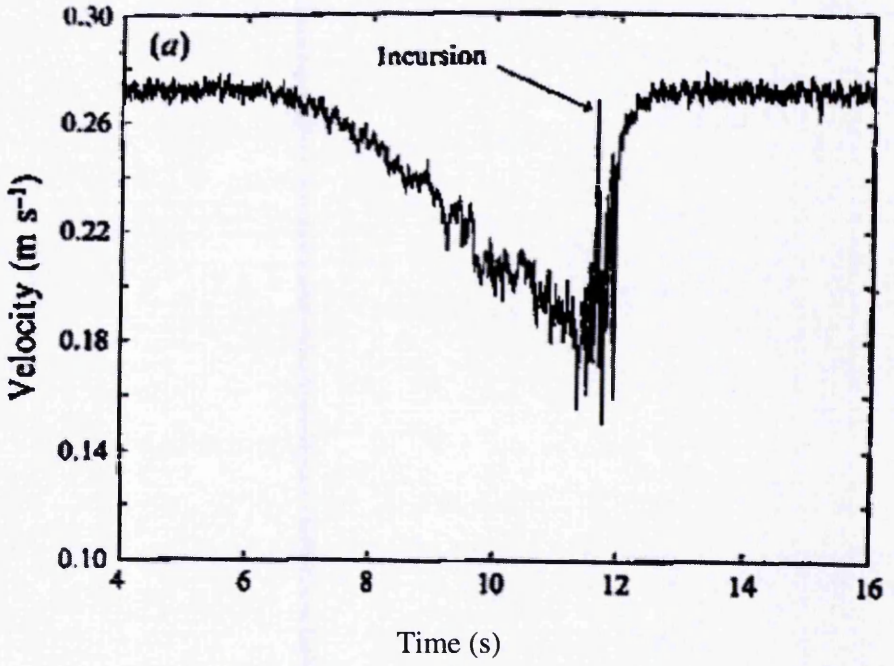

FIGURE 1.4. An LDV trace of the axial velocity in the centre of a pipe at one location as a puff passes. The Reynolds number of the pipe flow is 2300. The highest turbulent intensity is at the back interface of the puff, the turbulent intensity decays downstream approaching laminar flow. From Darbyshire & Mullin (1995).

In the experiments of Draad, Kuiken & Nieuwstadt (1998) the flow was disturbed at one location by injecting and removing fluid sinusoidally in time. For some distance from the disturbance generator the flow is laminar and the perturbation either grows or decays with distance. When the perturbations grows beyond some threshold amplitude the flow becomes turbulent. The place where the flow becomes turbulent is found to change rapidly with small changes to the amplitude of the disturbance. They characterise the stability of the flow in terms of the amplitude of disturbance that causes transition near the end of their pipe, 800 pipe diameters downstream. They calculated the value of γ in equation 1.3 to be between 1 and 2/3 depending upon the form of the disturbance.

Another experiment based upon a similar technique is reported in Eliahou, Tumin & Wygnanski (1998). They measured the flow profile downstream of a continuous disturbance that they applied to the flow. They compared the velocity profile of the flow when the amplitude of disturbance was too small to cause transition with the profile of flows which are about to undergo the transition to turbulence. It was found that the transition to turbulence was proceeded by the formation of a point of inflection in the flow. The evolution of the laminar flow was similar to the results of the numerical simulations of Zikanov (1996). Further experiments (Han, Tumin & Wygnanski 2000) revealed that after the formation of the point of inflection hairpin vortices would develop in the flow as found in boundary-layer transition.

A different approach was used in the experiment reported in Darbyshire & Mullin (1995). They used a disturbance generator that injected fluid into the flow for a finite amount of time. This produces a localised perturbation, in contrast to the global perturbations used in the investigations listed above which affect the entire downstream region of the flow.The Reynolds number used was between 2000 and 10000 and the disturbance would produce a single patch of turbulence. The disturbance amplitudes required for transition were comparatively large and turbulence formed within a few pipe diameters of the disturbance generator. The investigators observed whether or not this turbulence persisted or decayed to laminar flow further downstream.

The main difference between these two approaches is that in the first two experiments the flow is laminar for most of the flow domain of interest. In the last experiment the flow became turbulent rapidly and it was the evolution of this turbulent flow that was observed.

Dauchot & Daviaud (1995) performed an experiment on the stability of Couette flow by perturbing with the flow with a measured perturbation for a finite length of time. Their investigation was concerned with finding the stability of the flow at the lowest Reynolds number range that turbulence can be sustained. The disturbance amplitude, A_c, required to produce stable turbulent patches varies, at lowest Reynolds number for transition, as

$$A_c \propto (Re - Re_c)^{\Gamma} \tag{1.4}$$

The value of Re_c, the Reynolds number above which transition becomes possible, and Γ depend upon the type of perturbation used. The value of Γ must further depend upon the measure used to quantify the perturbation. Qualitatively the same behaviour was found in Darbyshire & Mullin (1995) in pipe flow. This equation, valid at Reynolds numbers close to Re_c and is similar in form to equation 1.3 which can only be valid for $Re >> Re_c$. However, the coefficients γ and Γ are found to be, in general, different.

Hence experiments upon pipe flow can be split into four different groups. There are experiments that use local perturbations and those that use global perturbations. These two groups of experiments are each further split up into two groups. Those experiments performed at Reynolds numbers where the stability is given by equation 1.3 and those at lower Reynolds numbers where 1.4 is valid.

1.8 Theoretical Stability Analysis of Developing Pipe Flow

The stability of developing pipe flow has received considerably less attention than that of Hagen-Poiseuille flow. Tatsumi (1952) was the the first researcher to calculate the linear stability of the developing pipe flow. He found that the entrance flow becomes linearly

unstable at Reynolds numbers higher than approximately 10000. Huang & Chen (1974) re-calculated the stability of the developing flow using the model of the entrance flow proposed by Sparrow et al. (1964) which was more accurate than the profile assumed by Tatsumi. They investigated the modes that have a azimuthal wave number of one. The minimum Reynolds number for neutral stability that they found was 19780. Later Gupta & Garg (1981) used a more accurate model of the flow profile as the basis for their calculations. This resulted in a new value of the minimum Reynolds number of 11700.

Sarpkaya (1975) investigated the linear stability of entrance flow using an experiment modelled on that used in Leite (1959). The results showed qualitative agreement with linear stability theory however the minimum Reynolds number for zero growth was found to be lower, at approximately 7000.

The linear instability gets weaker at increasing distances from the inlet but provides a window over which disturbances in the entrance flow can grow. If the disturbances grow too large then the flow can become turbulent before the laminar flow had time to become fully developed. For this reason the stability of the entrance flow is more important than the stability of the fully developed flow in many pipe flows of practical interest.

1.9 The Aims of this Investigation

In pipe flows it is found that the flow profile changes with distance from the inlet reaching Poiseuille flow only in the limit of large distance downstream. The stability of the entrance flow has been investigated using linear stability. The theoretical and experimental results indicate that the entrance flow is linearly unstable at some locations for Reynolds numbers above $\approx$ 10000. This does not however give any indication of the stability at lower Reynolds numbers.

This thesis details an investigation into the stability of developing pipe flow at the lowest Reynolds numbers at which transition can occur. The experiment is modelled on that performed by Darbyshire & Mullin (1995) and is summarised here. The stability

is defined in terms of the amplitude of disturbance required to produce sustained turbulence. Two types of disturbance are used, each disturbs the flow for a finite amount of time. Disturbing the flow for a finite amount of time localises the disturbance which is necessary for measuring the stability as a function of location. The flow features produced by the disturbances are not precisely known. However, at the amplitudes used the flow evolves rapidly and it may be assumed that a wide spectrum of modes are excited.

The next chapter contains a description of the apparatus and methods used in the experimental investigation. These include the construction of the pipe and mechanism used to draw the fluid through it. There is a discussion of the properties of the working fluid and the method used to visualise the flow. The design and operation of the two disturbance generators and the differences between them are explained in detail. The chapter closes with a description of the data acquisition and control systems which are used to run the experiment and extract data.

Chapter 3 gives an account of the properties of transition in the fully developed flow at $Re = 2170$. At this Reynolds number transition takes the form of turbulent puffs. The probabilistic nature of the production of puffs is discussed followed by the method of calculating the probabilities and their errors. The stability of the flow is characterised in terms of the amplitude of disturbance that results in a 0.5 probability of transition. The method of calculating the error in the amplitude is discussed along with the strategy to minimise the error. Finally a comparison is made between the speeds of the puffs produced in this experiment and those of measured by a previous researchers in pipe flow transition.

The methods used in chapter 3 are employed in an investigation of the stability of the entrance flow. The amplitude of disturbance required for a 0.5 probability of transition is measured at various locations in the developing pipe flow to obtain a stability curve. The shape of this stability curve is compared with that of the linear stability curve and the shape and properties of the developing flow profile.

The final results chapter concerns the change in the stability of pipe flow as the

Reynolds number is increased. First of all the trend in the stability of fully developed pipe flow at different Reynolds numbers is examined. Then the results of measuring the stability of the entrance flow at the different Reynolds number are presented. Finally the large numbers of experimental runs that were made throughout the different investigations were used to accurately calculate the average shape of the probability versus disturbance amplitude curve.

Chapter 2

Experimental Arrangement and Procedure

This chapter contains a description of the apparatus and procedures used to investigate the stability of pipe flow. The construction of the pipe and the equipment used to produce the flow are detailed and the calibration of this equipment is discussed. Two methods of disturbing the flow are explained along with the method of visualising the flow. The chapter finishes with a description of the methods used to automate the experimental procedure and take measurements.

2.1 The Pipe

The experimental apparatus is based upon that used previously by Darbyshire & Mullin (1995) and many of the details of the experiment are also published in their paper. The principal components of the experimental arrangement are shown schematically in figure 2.1. The pipe was constructed from 25, 150 mm long, transparent perspex sections each with an internal diameter of 20 mm. The sections fit together without any measurable gaps in the inner surface. These are the largest sections of tubing which can be machined

from solid blocks of perspex without distortion. The assembled pipe is held rigid along the entire length with supports mounted on a steel girder and is 188 pipe diameters long.

Darbyshire & Mullin (1995) found that all parts of the flow developed to within 6 % of the Hagen-Poiseuille profile after 70 pipe diameters at Reynolds number 2210. Hence 118 pipe diameters of Poiseuille flow are left to experiment upon. It is generally found (Fargie & Martin 1971) that in pipe flow at Reynolds numbers above 500 the developing flow profile, $\mathbf{u}$, varies with the Reynolds number, Re, and location down the tube, x, as

$$\mathbf{u} = \mathbf{u}(\mathbf{x}/\mathbf{dRe}) \tag{2.1}$$

where d is the pipe diameter. Using this result the maximum Reynolds number for which the flow evolves to within 94 % of the fully developed flow profile by the end of the pipe is 5900. This is close the conventional criterion for the development of pipe flow of $x/d = Re/30$.

The pipe was held at a 1.7^o angle to the horizontal in order to make it easier to fill with water and remove air bubbles. At the upper end of the pipe there was a storage tank and at the other end a piston that draws the water through the pipe. Using a large settling tank where the fluid is allowed to stand is the best way to ensure that the fluid that enters the pipe is free from disturbances. This was important for the development of the flow and repeatability of results. It was found that leaving the water for half an hour to settle between runs is enough time for visible fluctuations in the tank to decay and for repeatable results to be obtained.

Using a piston to draw the water through the pipe allowed a constant flow rate (constant Reynolds number) to be maintained during the transition to turbulence. The D.C. motor was powered by an EM100A motor controller connected to the piston via a ball screw. The rotation rate was calibrated using an RS optical shaft encoder (RS 341-597) which produces 500, 2.4 volt, pulses each revolution. The shaft encoder was fixed to rotate with the motor and the pulses counted using computer software which calculated

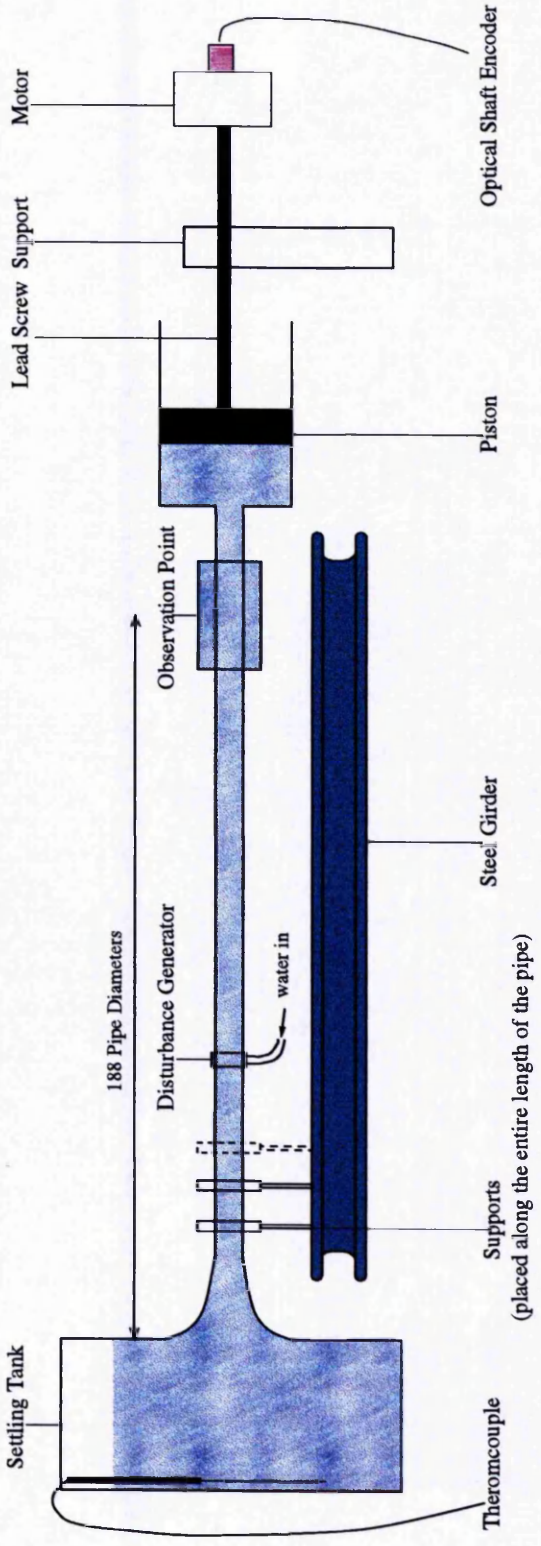

FIGURE 2.1. A schematic diagram of the main parts of the experimental apparatus, not to scale.

the angular velocity from the average time between pulses.

The Reynolds number can be calculated from the speed of the motor through knowledge of the pitch of the lead screw, S, and the ratio of the cross sectional areas of the piston, A, and the pipe $\pi d^2/4$. The formula for the Reynolds number of the flow in terms of the angular frequency of the motor is,

$$\begin{aligned} Re &= \frac{\overline{u}d}{\nu} \\ &= \frac{4AS}{\nu\pi d} f \\ &= 2280f \pm 1\% \end{aligned} \tag{2.2}$$

where f is in Hz. The 1 % error comes from the measurement of the viscosity of water which was measured using a suspended level viscometer at 20 °C. The viscosity of the water at the temperature of the experiment was calculated from this measured viscosity, ν_{20}, using the formula

$$log_{10}(\nu) = \frac{1.327(20-T) - 0.001053(T-20)^2}{T+105} + log10(\nu_{20}) \tag{2.3}$$

This empirical relationship was taken from (Weast 1980) and is valid in the temperature range 15 °C − 30 °C. It can be seen from the plot of equation 2.3 in figure 2.2 that, at 20 °C, a one degree change in the temperature changes the viscosity by 3 %. Two steps were taken to minimise the effect of temperature on the experiment. First the laboratory is air-conditioned to maintain a constant temperature of 19 °C ± 1 °C. Second the speed of the motor is adjusted for the viscosity calculated at the temperature of the water in the tank. The temperature is measured and recorded before each run using a thermocouple. This thermocouple was calibrated against the same mercury thermometer used in the viscosity measurements.

The flow rate varies linearly with the voltage applied to the motor controller for Reynolds numbers up to and in excess of 20000 as shown in figure 2.3. In an experimental run the control voltage is increased smoothly from zero following a half Gaussian profile up to the required value. By plotting the rotation rate of the motor against the

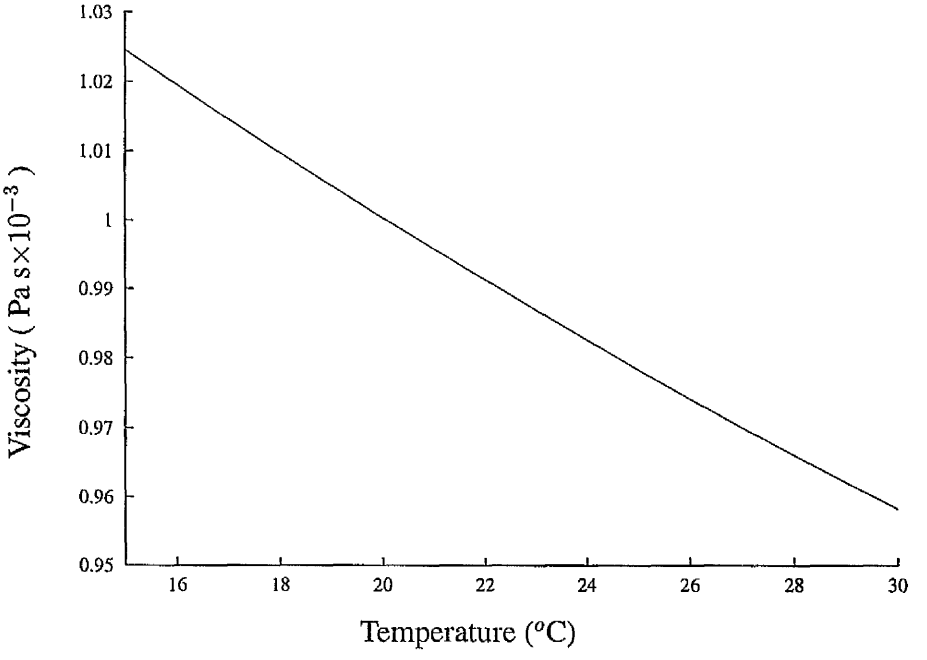

FIGURE 2.2. The variation of the viscosity of water with temperature plotted using equation 2.3

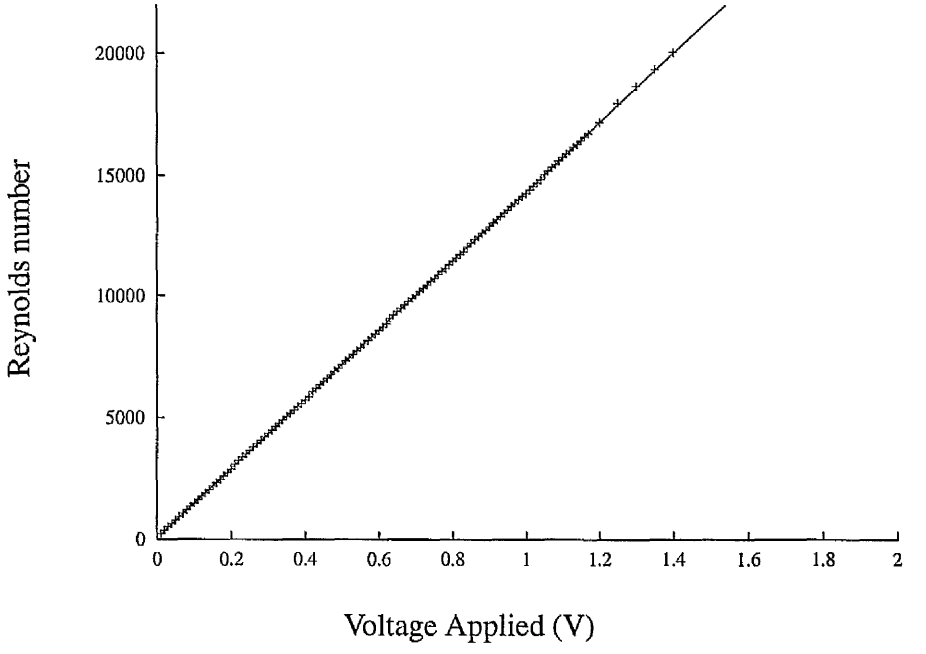

FIGURE 2.3. Graph of Reynolds number of the pipe flow against the voltage applied to the motor controller plotted with a linear fit. From this graph it can be seen that the response of the motor is linear beyond $Re = 20000$. This graph was constructed from data from an optical shaft encoder in conjunction with the formula in 2.2.

control voltage it was found that the speed of the motor follows this Gaussian profile up to reasonably high Reynolds numbers. Such a plot is presented in figure 2.4 for one of the highest Reynolds numbers. There is some lag in the flow speed at this Reynolds number but there is no overshoot and the flow has reached the steady state within 3 seconds.

Under these conditions the flow in the pipe is laminar at the highest Reynolds number the experiment is calibrated for, that is 2×10^4.

2.2 Disturbance Generators

Because pipe Poiseuille flow is believed to be linearly stable at all Reynolds numbers, under controlled conditions, the flow remains laminar until perturbed. There are two disturbance generators that are used in this investigation. They both work by injecting

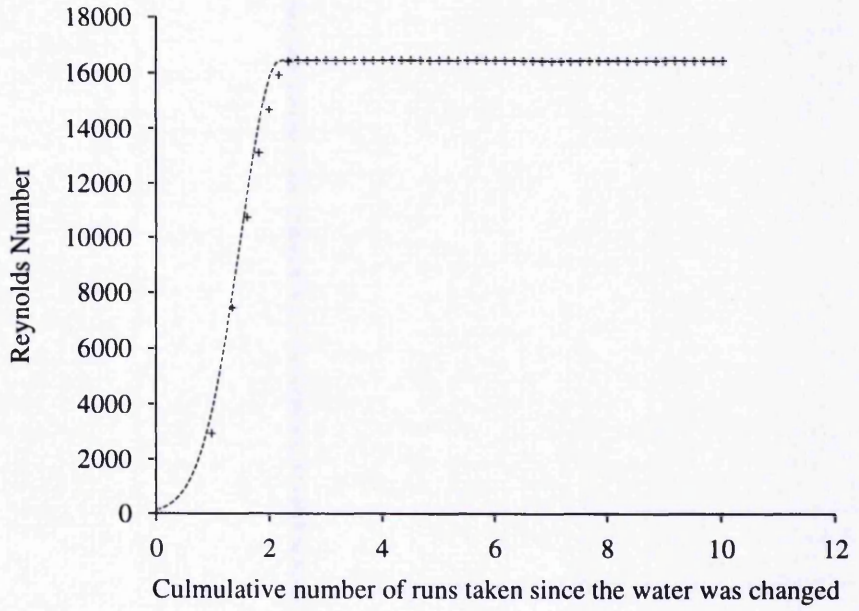

FIGURE 2.4. The Reynolds number of the flow against time during an experimental run. The points are the rotation rate of the motor measured using an optical shaft encoder using one pulse per revolution. The line is the voltage that is applied to the motor controller. The control voltage and the rotation rate of the motor have been converted into Reynolds numbers via calibration data in figure 2.3 and equation 2.2 respectively. The Reynolds number increases smoothly from zero reaching the intended steady Reynolds number with no significant over shoot. It is maintained at that constant level until the experimental run is complete. The rotation rate was measured with an optical shaft encoder using one pulse per revolution.

water into the flow but perturb different parts of the flow. The one-jet disturbance was designed to disturb the centre of the flow and does this by injecting a single jet a perpendicular to the pipe wall. The six-jet disturbance perturbs the region of flow near the wall by injecting fluid at a small angle to the wall. In order to disturb the flow over the entire neighbourhood of the wall six-jets where used, equally spaced around the pipe's circumference.

When these disturbance generators are used to disturb the flow at Reynolds numbers between 2170 and 4000 either a stable turbulent patch is produced or the flow evolves back to Poiseuille flow. There is a range of disturbance amplitudes and Reynolds numbers for which the transition is probabilistic. Most of the experimentation involved measuring the probability of transition at different parameters. In the next two sections the design and operation of the disturbance generators are discussed in detail.

The One-jet Injection Disturbance

This disturbance is effected by injecting water into the middle of the pipe from a 3 mm length cylindrical hole of diameter 2 mm. A schematic diagram of the disturbance generator and a picture of it in use are shown in figures 2.5a) and 2.5b). The fluid enters the pipe flow perpendicular to both the wall and the direction of the main flow. As shown by the pattern of ink injected into the pipe the fluid reaches the centre of the pipe.

A picture of the pump apparatus is shown in figure 2.6. The pump is controlled by a lever which is moved by a DC motor. When the lever is pushed into the pump assembly water is ejected out of the top outlet. As the lever returns a spring provides the restoring force which pulls the water back into the pump through the lower inlet. The outlet is connected to the pipe via a rigid tube and the inlet to a reservoir of water.

The amplitude of the disturbance is altered by changing the lever's range of travel. The apparatus is set up so that the range of travel can be adjusted to an accuracy of 0.05 mm by means of a vernier scale. The motor is always turned at the constant rate of 0.409

a)

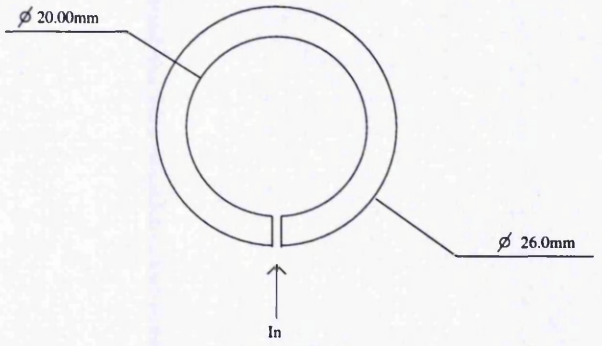

b)

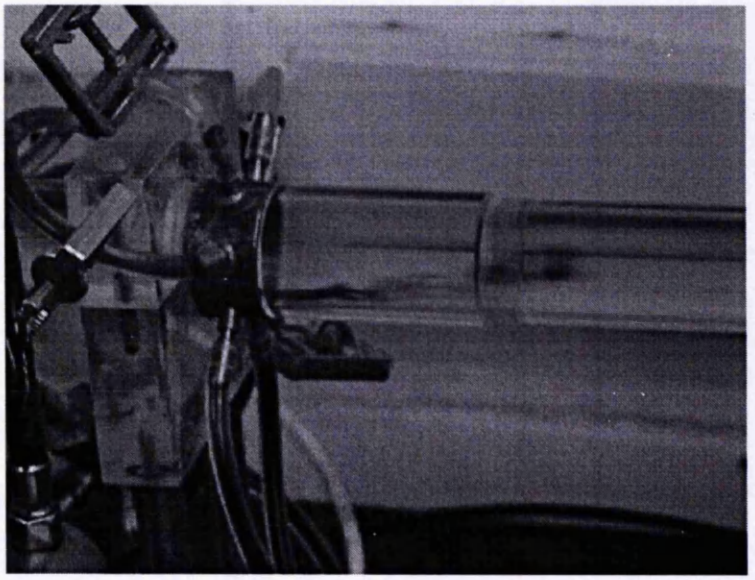

FIGURE 2.5. The one-jet disturbance generator. a) A schematic diagram of the disturbance generator. b) A picture of the disturbance generator in action. Only the tube at the bottom of the disturbance generator carries fluid into the pipe, all of the other tubes are clamped closed. When the picture was taken the injected fluid was coloured with ink to reveal the extent of the flow of the injected fluid.

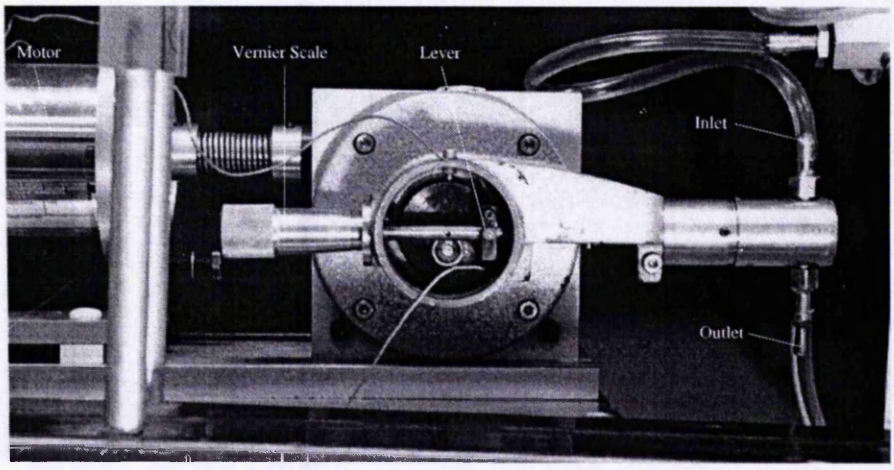

FIGURE 2.6. The mechanism used to pump water into the experiment, including the motor, the vernier scale and the inlet and outlet pipes.

Hz, the same value used by (Darbyshire & Mullin 1995). The rate of fluid injection rapidly reaches a maximum when the bearing comes in contact with the lever. The rate of flux then reduces to zero as the bearing rotates to its maximum horizontal position.

The Six-jet Injection Disturbance

A schematic diagram and a picture of the disturbance generator are shown in figures 2.7 a) and b) respectively. The apparatus used to pump the water, and hence also the mass flux of water, is the same as that for the one-jet disturbance. The main difference between the disturbance generators is that the fluid is injected into the flow through thin tubes, 0.3 mm in diameter. The holes are oriented so that the fluid enters the flow at an angle of 32^o to the wall so that the injected fluid stays close to the pipe wall. It also means that some net vorticity is added to the flow, the one-jet disturbance does not contribute any net vorticity. The fluid is injected though six holes giving the disturbance an azimuthal wave number of six.

2.3 Flow Visualisation

finite disturbances were used to find its stability limits. The state of the flow in the pipe was made visible by adding flow-visualisation material to the water. Three different materials were tested for suitability as flow visualisation, Mearlmaid, ink and Kalliroscope.

2.3.1 Mearlmaid Flow Visualisation

Mearlmaid is a commercial product used in the manufacture of cosmetics and produced by Engelhard Inc. The solution contains small highly reflective flat particles extracted from fish scales. The flakes reflect more light from their flat sides than from their thin perimeter. Because the flakes tend to become aligned along streamlines the flow struc-

(a)

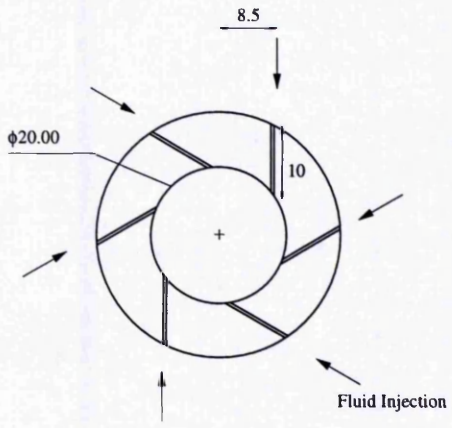

(b)

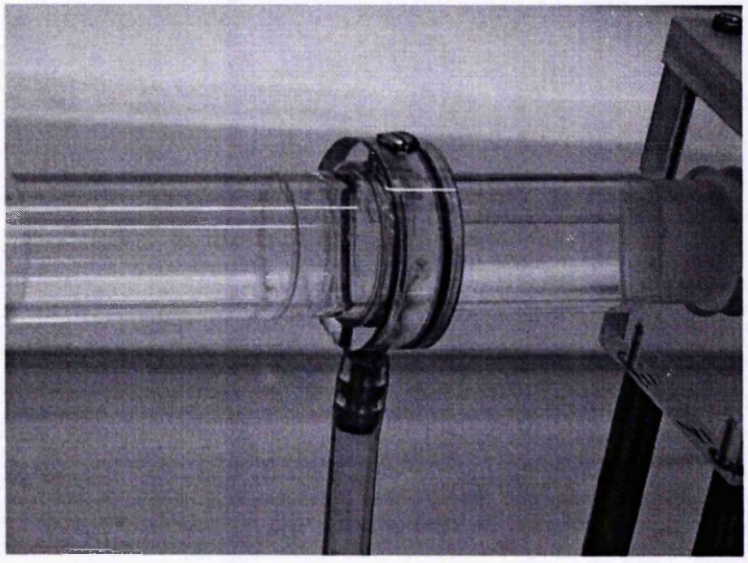

FIGURE 2.7. A picture and a schematic diagram of the six-jet disturbance generator. a) All of the dimensions are in millimetres. Water is injected into the pipe through all six holes when water is pumped into the jacket. The angle between the holes and the tangent to the walls is 32^o. b) The jacket around the pipe is filled with water from the hose underneath the pipe.

tures are revealed as patterns of light and dark. The patterns have the best contrast when the flow is illuminated with a thin light sheet perpendicular to the line of sight.

Mearlmaid is first mixed with a small amount of water, the solution is then filtered through two layers of muslin before being added to the water in the experiment. The 35 l of water in the apparatus required 0.3 g of Mearlmaid for the patterns to be visible to the naked eye at Reynolds numbers of several thousand. The flakes have a density slightly greater than that of water and so tend to settle at the bottom of the tank, where the flow velocity is always low. This is minimised by drawing water from the tank through the pipe and back three times after each run. When this is done the flakes remain in suspension for up to six days.

To test the effect of Mearlmaid upon the flow the probability of transition was measured at one set of parameters with different amounts of Mearlmaid in solution. The parameters were, a disturbance amplitude of 173 mm^3 using the six-jet disturbance generator, 29.6 pipe diameters from the inlet. The first 0.5 g of Mearlmaid was added to the water; this stayed in solution for six days. Afterwards the pipe was cleaned, the water was changed and 0.2 g of Mearlmaid was added to the water. Two days later this was repeated with 0.3 g and finally 0.5 g was used four days after this. The graph of the measured probability of transition after different numbers of runs have been carried out is plotted in figure 2.8 a). It can be seen that the probability of transition is not correlated with the concentration of Mearlmaid in solution.

2.3.2 Ink Flow Visualisation

Ink is first injected into the pipe near the wall while the water is stationary. When water is drawn through the pipe the ink is stretched out downstream into a line along the wall of the tube. If the flow remains laminar the line of ink retains its shape. However turbulent flow disturbs the ink mixing it over the whole cross section of the pipe. The ink that was used is called "Quink" and is sold by Parker.

a)

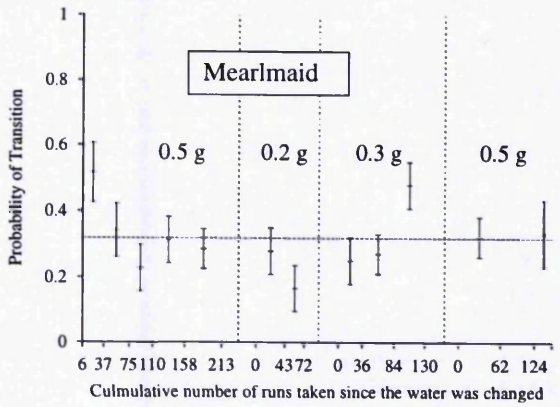

b)

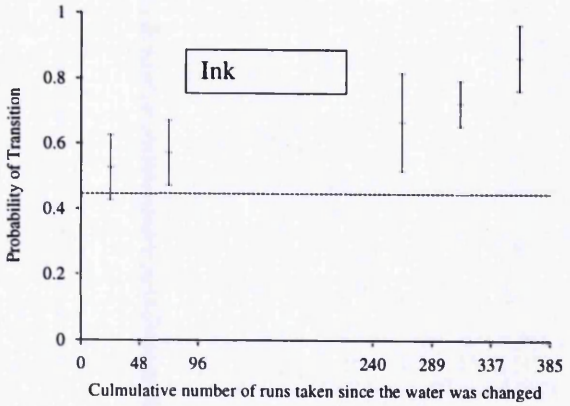

c)

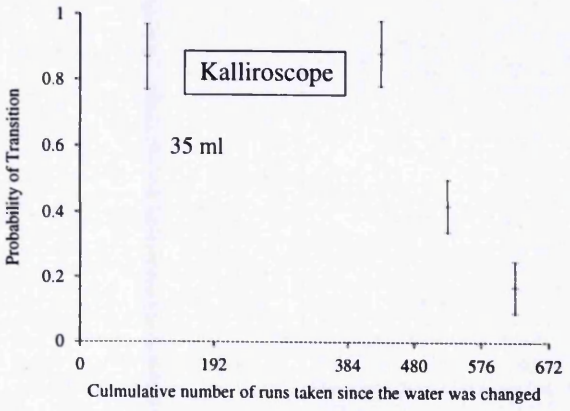

FIGURE 2.8. Graphs of the probability of transition for repeated experimental runs using different types of flow visualisation. In each case the experiments were also performed using Mearlmaid as flow visualisation and the measured mean probability is added as a horizontal dotted line for comparison. a) Mearlmaid b) ink c) Kalliroscope

This method was used to measure the probability of transition at a constant disturbance amplitude of 268 mm^3 over several days. The disturbance used was, again, the six-jet disturbance generator at 29.6 pipe diameters from the inlet. The probability of transition after different numbers of runs is plotted in figure 2.8 b). The probability was later measured at these parameters using Mearlmaid, the mean probability of transition when Mearlmaid was used is shown for comparison.

While the probability of transition was initially consistent with the Mearlmaid result, the probability of transition increased as more experimental runs were made. This increase in the probability is due to the addition of ink before each experimental run. Confirmation of this came from adding a large amount of ink to the water and finding the probability of transition to be one.

2.3.3 Kalliroscope Flow Visualisation

Kalliroscope is a solution similar to Mearlmaid but contains short length polymers that allow the particles to stay in suspension for longer. It is made and distributed by the Kalliroscope Corporation.

Once again the experiment was run repeatedly using the six-jet disturbance generator, 29.6 pipe diameters from the inlet. This time the amplitude used was 115 mm^3. A graph of the probability of transition calculated after the completion of different numbers of runs is given in figure 2.8 c). Again the probability was also measured at the same parameters using Mearlmaid as flow visualisation.

The probability of transition is initially much greater than that for Mearlmaid but reduces as more runs are completed. Unlike ink flow visualisation, Kalliroscope is not added to the water before each experimental run and its concentration does not change with time. The cause of the change must be due to evaporation or degradation of a component of the material. Such degradation has been found in polymer solutions that are subject to shear. For example Kim *et al.* (2000) investigated the change in the length

of polymers in turbulent flow and found degradation on time scales of tens of minutes.

2.3.4 Conclusions

Mearlmaid is the only flow visualisation out of the three tested that did not appear to change the stability of the flow. For this reason all of the experiments reported throughout the rest of this thesis used Mearlmaid.

As the ingredients that are used in the ink and Kalliroscope are not ready available it is not possible to identify the substances that are effecting the flow. The results show that the presence of these materials is to reduce the stability of laminar pipe flow, hence increasing the number of transitions.

2.4 Control

The whole process of periodically starting runs, controlling the equipment and recording the data was automated so that runs could be made 24 hours a day. The equipment was controlled using a computer with a Data Translation DT3001 analog to digital card. The DT3001 card has two analog outputs, 8 analog inputs and 8 digital outputs. The analog input/outputs have $2^{16} = 65536$ digital levels equally spaced between ± 10 volts. The two analog outputs were used to control the flow speed and the disturbance generator. The inputs measured the position of motor used for the disturbance generator and the temperature.

The flow patterns were recorded with a Pulnix CCD camera with a resolution of 768 by 576, interlaced, at a frame rate of 25 frames per second. Individual frames were recorded as required using a frame grabber connected to the computer.

The camera viewed a 0.1 m length of pipe through a cuboidal water jacket . The water jacket minimised the optical distortions caused by viewing the fluid through the cylindrical pipe. A frame was recorded at time intervals equal to 0.1 m divided by the

a)

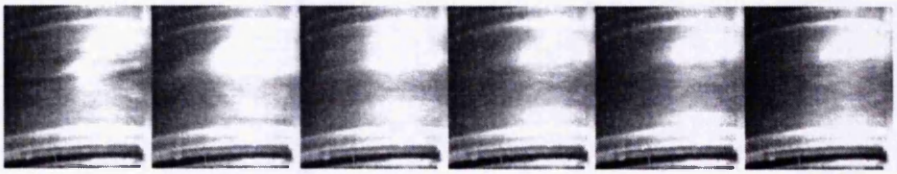

b)

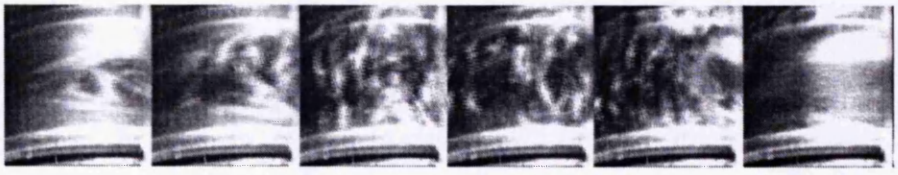

FIGURE 2.9. Images from two consecutive runs half an hour apart both at a Reynolds number of 2170. a) In this experimental run a puff had not been produced by the disturbance b) Here a puff has persisted and the weak front and welldefined back interface can be made out.

mean flow velocity. This frame rate was chosen because equilibrium puffs, which are the focus of the next two chapters move at the mean flow rate. Capturing images in this way and concatenating them together allows information about the puff, like its length to be measured.

For the purpose of viewing the images it is easier to see turbulent flow features if the width of the image is reduced by a factor of 10 as the patterns appear less diffuse. A pair of such images are shown figure 2.9. The top image is laminar flow with a small remnant of a turbulent patch that decayed. The lower image is a stable turbulent puff showing the characteristic diffuse downstream interface on the left with the sudden relaminarisation on the up-stream interface. Although it is sometimes possible to see decaying turbulent flow features, like that in figure 2.9 a), these are always much smaller than stable turbulent patches. The factoroften reduction in the width of the images makes the flow patterns appear more elongated than they really are.

Chapter 3

Measures of the Stability of Pipe Flow at Reynolds number 2170

This chapter concerns the effects of perturbing Hagen-Poiseuille flow and introduces the method by which quantitative measurements of the stability of the flow were made. The chapter focuses upon the nature of transition at Reynolds number 2170, near the low-Reynolds-number limit for which transition can occur. First the probabilistic nature of the transition is introduced and then the quantities used to characterise the stability of pipe flow are discussed. Next the procedure used to calculate these quantities and their errors is discussed. There is a short description of an investigation into the measurement of the time required for the transients to decay. Finally the speeds of the puffs are compared with the those in the published literature.

3.1 The Effects of Perturbing the flow

The flow is perturbed using either one of the disturbance generators described in section 2.2. At Reynolds numbers where puffs and slugs are stable, (c.f. Introduction section 1.6) the transition to turbulent flow will take the form of a single puff or slug. The two

parameters that govern whether a patch of turbulence is stable or not are, the Reynolds number and the form of the disturbance.

The experiments of Darbyshire & Mullin (1995) showed that the transition to turbulence in pipe flow is sensitive to form of the applied perturbation. The result of this is that the long-term evolution of two perturbations, in two different experimental runs performed at measurably the same parameters can be different. Hence for many ranges of parameters it is only possible to measure the probability that a puff will be produced as a result of a perturbation.

There are two different causes of this sensitivity which we will discuss briefly here and return to later in the light of the experimental findings. There is sensitivity to initial conditions which is a feature of the transition to turbulence in many shear flows (Eckhardt & Mersmann 1999). This is caused by the basin of attraction between the laminar and turbulent states having a fractal-like shape. Tiny changes to the experimental conditions can place the system across the boundary of one basin of attraction and into another. The probability of transition at a set of parameter is given by the proportion of parameter space taken up by basins of attraction of the laminar and turbulent states.

The transition to turbulence will be sensitive to the form of the disturbance if the requirements for a disturbance that can initiate transition are complicated. It was mentioned in section 1.4 that the amplification of disturbances may require the interactions of a large set of modes numbering of order 100. It would be expected that if some of this large number of modes are not well represented in the disturbance's spectrum then experimental noise will become important in deciding the evolution of the disturbance. This would also explain the probabilistic nature of the transition to turbulence.

The probabilistic nature of the transition to turbulence in pipe flows is not restricted to experiments where the flow is perturbed over a finite amount of time. Investigations of pipe flow transition that involved disturbing the flow continuously have found the probabilities occurring in different ways. For example both (Wygnanski & Champagne 1973) and (Reynolds 1883) disturbed the flow continuously. In (Wygnanski & Champagne

1973) it was found that turbulent patches formed intermittently in time while (Reynolds 1883) observed patches forming at different downstream locations.

It is important in the present experiment that measurements are made far downstream from the disturbance so that transients have had time to decay. If the state of the flow is measured too close to the disturbance generator the properties of the flow will be dependent upon the distance from the disturbance generator where measurements were made. A later section in this chapter describes the investigation performed to find the lifetime of transients.

Contained in figure 3.1 is a graph of the probability of sustained transition against disturbance amplitude at a Reynolds number of 2170 for the two types of controlled disturbance. For small disturbances the probability of transition is zero. Beyond some threshold, the probability, p, increases monotonically with the disturbance amplitude, A, until $p = 1$.

The shape of the probability curve, $p(A)$, is the subject of an investigation outlined in section 5.4. It is advantageous to approximate the shape of the probability versus amplitude relationship with three straight line fits. The equations of these fits for low, intermediate and high disturbance amplitudes are,

$$\begin{aligned} p(A) &= 0 && \text{small } A \\ p(A) &= aA + b && \text{intermediate } A \\ p(A) &= 1 && \text{large } A \end{aligned} \tag{3.1}$$

The line that fits the data points in the probabilistic region ($p \neq 0$ or 1) can be defined in terms of the amplitude for which $p = 0.5$ and the width of the region. These two quantities will be referred to as the critical disturbance amplitude, A_c and the probabilistic width, W, respectively. They are related to the gradient of the line, a and its intercept, b, by the relations.

$$A_c = \frac{0.5 - b}{a} \qquad W = \frac{1}{a} \tag{3.2}$$

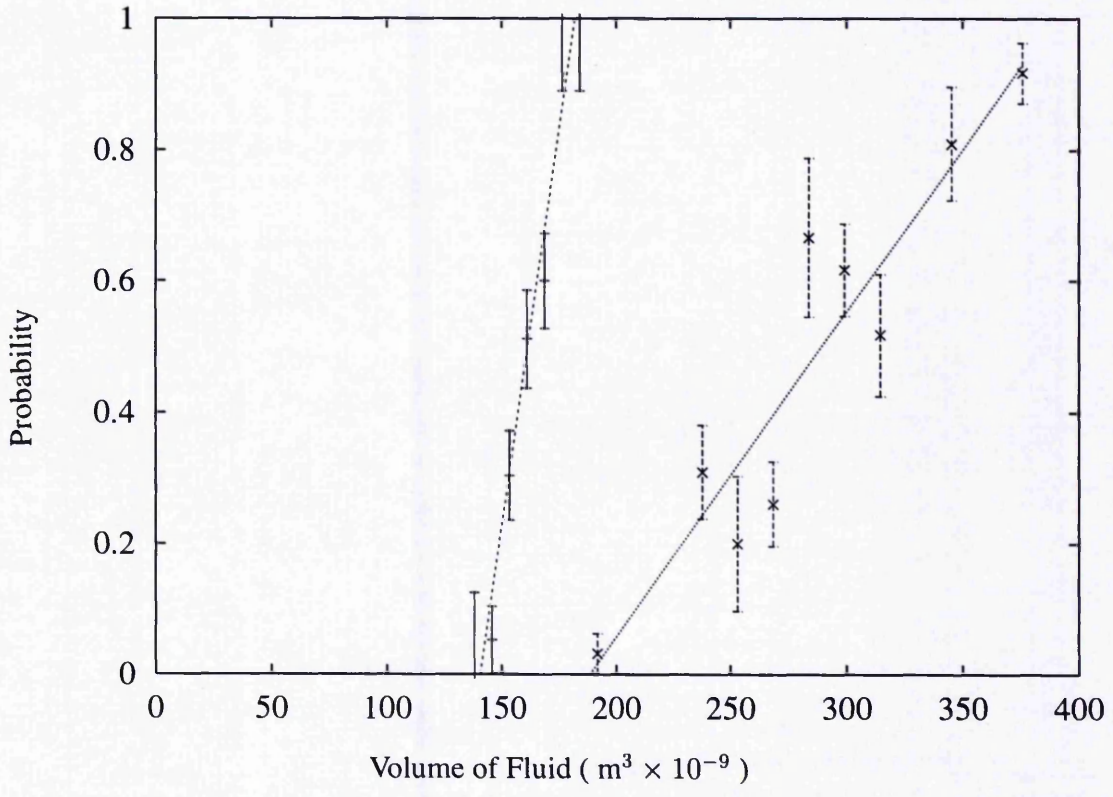

FIGURE 3.1. The probability of transition at different values of the disturbance amplitude for the six-jet (horizontal crosses) and one-jet (diagonal crosses) disturbances.

Each point in the graph was the result of approximately 30 runs. The plots for the one-jet and six-jet disturbance generators contain 283 and 181 experimental runs respectively. The errors on the probabilities are statistical errors due to calculating the probabilities from a finite number of measurements. Section 3.2 concerns the calculation of these errors and how they determine error in A_c.

It can be seen from figure 3.1 that the form of the disturbance changes both the critical disturbance amplitude and the probabilistic width. The disturbance amplitude required to cause transition is less for the six-jet disturbance than the one-jet disturbance. This means that the flow is more unstable to the perturbation produced by the six-jet disturbance generator. As discussed in section 2.2 the six-jet disturbance disturbs the wall layer of the flow while the one-jet disturbance disturbs the inner region. This implies that it is more difficult to cause transition by disturbing the central core of the flow perhaps because the disturbance is stretched out by the fastmoving flow.

It can also be seen in figure 3.1 that the size of the probabilistic region is smaller for the six-jet disturbance. This feature is preserved even if the amplitude scale is normalised with respect to the critical disturbance amplitude.

3.2 Calculating Critical Amplitudes

The critical disturbance amplitude and the probabilistic width are calculated from the straight line that is fitted to the points in the probabilistic region. The fit is made using the least-squares fitting program built into GNUPLOT. The rest of this section concerns the calculation of the error on the critical disturbance amplitude.

Throughout this thesis the probability of transition is measured by repeating experimental runs at the same set of parameter of values. The definition of the probability of

transition is

$$p = \left.\frac{t}{N}\right|_{lim(N\Rightarrow\infty)} \tag{3.3}$$

where t is the observed number of transitions and N is the number of experimental runs. When N is finite the best estimate of the probability of transition is still given by that ratio but the value of the probability has an uncertainty. The probability,$P(t,N,p)$, of recording a certain number of transitions in a given number of runs is given by the binomial distribution.

$$P(t,N,p) = p^t(1-p)^{N-t}\frac{N!}{t!(N-t)!}$$

The uncertainty in the probability of transition is calculated using the *Clopper-Pearson confidence* limits (Barlow (1989) page 132). Here the binomial distribution is used to calculate the likelihood that p is between an upper and lower limit. Setting this likelihood equal to the confidence level, C, results in these equations for the upper and lower limits, p_+ and p_- respectively,

$$\begin{aligned}\sum_{r=t+1}^{n} P(r,N,p_+) &= \frac{1+C}{2} \\ \sum_{0}^{t-1} P(t,N,p_-) &= \frac{1+C}{2}\end{aligned} \tag{3.4}$$

The difference between p and the maximum or minimum limit, which ever is greater, is used as an error on p. A 68 % confidence level is used as this is the same confidence that a measurement is within one standard deviation of the true value when the errors are Gaussian distributed. An alternative method of calculating the uncertainty would have

N	t	Error from Clopper-Pearson confidence limits (equation 3.4)	Error from the standard deviation ($\frac{\sqrt{p(1-p)N}}{N}$)
40	20	0.090	0.079
40	1	0.080	0.025
40	0	0.045	0.00
20	10	0.13	0.11
20	1	0.11	0.049
20	0	0.087	0.00
10	5	0.19	0.16
10	1	0.19	0.095
10	0	0.17	0.00
5	2	0.30	0.219
5	1	0.32	0.18
5	0	0.31	0.00

Table 3.1. Some examples of errors calculated using the standard deviation of the binomial distribution and Clopper-Pearson confidence limits. All of these examples are for probabilities of half or less, however the error is the same for probabilities of p and $1-p$.

been to use the standard deviation of the data. However this fails when the results are either all transitions or contain no transitions so that the standard deviation is zero.

Errors calculated using the Clopper-Pearson confidence limits and the standard deviation for different values of t and N are listed in table 3.1. When N is large and $p = 0.5$ the results of the two methods differ by approximately 10 %. The uncertainty in p has a $1/\sqrt{N}$ dependence so that four times as many experimental runs are required to half the uncertainty. However when p is close to zero or one, the standard deviation substantially under estimates the uncertainty. It can be seen from table 3.1 that when p equals zero the error is approximately proportional to $1/N$.

Now that the errors on the individual probabilities have been calculated it is possible to estimate the error on the value of A_c. In principle it is possible to calculate the error directly from equation 3.1 using the errors on the fit parameters. This is complicated, however by the fact that the fit parameters a and b are correlated. A simpler expression for the errors comes from shifting the origin to the mean point of the data. This reduces

the fit to a one-parameter fit as b is now zero. Here the fact that the mean of the data is a point on the line of best fit has been used. This result is best known for the case when all of the points have equal weight (equal errors), for example Barlow (1989) page 101. However it is always possible to reduce weighted data points into an equally weighted data set by splitting each result into a number of points proportional to its weight.This will produce one or more points for each value of A, the error on which is greater the error on the original point. Calculating the mean amplitude, $\overline{A}$, and the mean probability, $\overline{p}$ from this new data set defines a point on the line of best fit.

The error on this point is just the standard deviation of the mean of the probability,

$$(\Delta\overline{p})^2 = \frac{1}{\sum_m 1/(\Delta p_m)^2}$$

The sum can either be over the different points in the new data set or over all of the measured probabilities, the standard deviation is the same. It is necessary to calculate the error on the points in the new data set. The errors on the points at each value of A when added in quadrature must equal the total error on the measured data point. Hence the error on the new data points, σ, can be calculated from any measured data point using

$$\sigma = \sqrt{M}\Delta p$$

where M is the total number of points that the original data point was divided into.

The error on A_c is now in two parts, the error from extrapolating from the mean point due to the uncertainty in the gradient and the error on the coordinates of the point itself. As the location of the mean point is not correlated with the gradient these two errors can be added in quadrature. The error on A_c is

$$(\Delta A_c)^2 = (\frac{(\overline{p}-0.5)\Delta a A_c}{a^2})^2 + (\frac{\Delta\overline{p}}{a})^2 \tag{3.5}$$

The error on the gradient, Δa is calculated using the formula from Barlow (1989) page 101.

$$\Delta a = \sqrt{\frac{\sigma^2}{N(\overline{A^2}-\overline{A}^2)}} \tag{3.6}$$

(3.7)

When calculating the mean and the gradient only points that are in the probabilistic region can be used. Points with probabilities of zero or one and which are outside the probabilistic region are no use for estimating A_c. Choosing the points that should be included requires estimating the equation of the line of best fit using the data points that are certainly in the probabilistic region. This is used to make a first estimate of the size of the region. Calculating the gradient of the line of best fit from all of the points in this region is used to finally decide which points are and are not to be included.

It is evident from equation 3.5 that lower errors can be achieved if the data points are chosen so that $\overline{p}$ is close to 0.5. This is equivalent to $\overline{A} \approx A_c$. It is often possible to choose the values of A for which the probabilities are measured as the experiment progresses in order to achieve this. Doing this can make the first term in equation 3.5 small compared with the second term.

3.3 The lifetime of Transients

As was discussed in the Introduction (section 1.6) puffs produced at Reynolds numbers of around 2000 propagate at constant size and are called equilibrium puffs. It seems likely that once generated these puffs are stable for all time. However it is not possible to prove this with a finite length pipe.

As reported in Darbyshire & Mullin (1995) near to the disturbance generator a turbulent patch is always formed when a disturbance is added close to the critical disturbance amplitude. It is hard to tell which patches will evolve into long lived turbulent puffs or slugs and which decay by observing them before 25 pipe diameters from the disturbance. In this way the system appears deterministic close to the disturbance generator and the true probabilistic nature shows itself only further downstream. Measuring the probability of producing a stable puff requires knowledge of the distance over which transients decay.

Here the investigation made to find the distance over which all transients decay. The

Re	Distance from the Disturbance Generator				
	0	15.7	22.7	57.7	102.7
2170	1	1 ± 0.037	0.9 ± 0.2	0 ± 0.045	0

Table 3.2. The probability that a puff produced by the one-jet disturbance generator that decayed had not relaminarised at different distances. The probability reduces with distance reaching zero at or before 58 pipe diameters. The total number of transients counted in this investigation was approximately 100

flow is observed at 102.7 pipe diameters from the disturbance and at some intermediate position. It is assumed for the present that 102.7 pipe diameters is far enough for all transients to decay. This assumption will be tested later. The assumption allows turbulent patches that remain until 102.7 pipe diameters to be labelled as stable turbulent puffs and those that do not to be labelled transients.

Let the probability that a transient had not decayed at that intermediate point, x pipe diameters from the inlet, be denoted by $p(x)$. This is equal to

$$p(x) = \left. \frac{s(x)}{s(x)+r(x)} \right|_{lim(s(x)+r(x) \Rightarrow \infty)} \tag{3.8}$$

Here $s(x)$ is the number of transients observed at point x and $r(x)$ is the number of runs were the flow relaminarises before reaching x. Note this investigation concerns only transients, the $\approx 50\%$ of turbulent patches that develop into stable puffs do not feature in the equation.

These arguments imply that the probability of finding a transient at the disturbance generator is one, while the probability at 102.7 pipe diameters is zero. The probabilities of finding transients at three other locations were measured at Reynolds number 2170 using the one-jet disturbance generator. The results are tabulated in table 3.2. The number of transitions reduces with distance from the disturbance reaching zero at 58 pipe diameters.

The assumption that all transients disappeared before 102.7 appears to be justified as the number of turbulent patches does not change between 58 and 102.7 pipe diameters.

In this we are assuming the rate of decay of turbulent puffs changes monotonically with distance. Another possible flaw in this argument is that the rate of decay may not have decreased to zero by 58 pipe diameters but some small value. Over 50 pipe diameters there may be no appreciable decay but from 103 to ∞ it may be considerable.

What is being assumed is that far from the disturbance generator the rate of decay decreases exponentially with distance. This is type of decay implies that the probability of decay for a transient at some location is independent of that location.

Supporting evidence of this comes from the properties of turbulent patches in plane Couette flow. Plane Couette flow is the flow of fluid between two large parallel plates moving relative to one another. If the walls move at the same speed but in opposite directions the mean flow rate is zero. In these conditions turbulence patches formed in the flow remain on average stationary. Examining the lifetimes of these patches Dauchot & Daviaud (1995) found that while many patches did not decay the rate of decay amongst those that did was exponential. It is assumed here that the life times of turbulent puffs has qualitatively the same behaviour.

It would seem that in order to be confident that transient turbulent patches are not counted the observation point should be more than 58 pipe diameters from the disturbance. This investigation was performed using the one-jet injection disturbance. As the turbulence is observed to fill the pipe cross section in less than 10 pipe diameters the results for the six-jet disturbance should be similar. Throughout the rest of this investigation the minimum distance of the observation point from the disturbance generator was 74.8 pipe diameters for Reynolds numbers of 2170.

3.4 Comparison of the speed of measured propagation of puffs with those reported in published works

In this section the speeds of the interfaces of puffs produced in the current experiment at Reynolds number 2170 are compared with those reported in Lindgren (1969). The graph of the speeds of the two interfaces against Reynolds number presented in Lindgren (1969) is reproduced in figure 3.2.

It is found that as the Reynolds number goes to infinity the speed of the back interface approaches zero, while the speed of the front interface increases. At some Reynolds number close to 2000 the two interfaces have the same speed and so the patch remains the same size. At lower Reynolds numbers the patches shrink, ultimately giving way to laminar flow.

It can be seen from the graph in figure 3.2 that there is a range of Reynolds numbers over which the front and back interfaces propagate at the same speed. These are the equilibrium puffs described in Wygnanski & Friedman (1975). The speed of propagation of these flow features is close to the mean flow velocity. This is what would be expected for the speeds of the interfaces in the current experiment at $Re = 2170$.

In the experiment the speed of the turbulent-laminar interfaces in puffs were measured by recording the flow at two reference points (69 and 112 pipe diameters from the disturbance generator). The flow was recorded at the two locations with two CCD cameras. By examining the recorded frames the times taken for the interfaces to get from the disturbance generator to the reference locations were calculated.

One difficulty with determining the speeds of the interfaces is that the puffs' shape changes due to their internal turbulent motion. This effect on the measurement was minimised by choosing a representative point for each interface that remained approximately stationary with respect to the time average shape of the puff. For the back interface this was the point on the interface in the middle of the pipe. The best reference location for

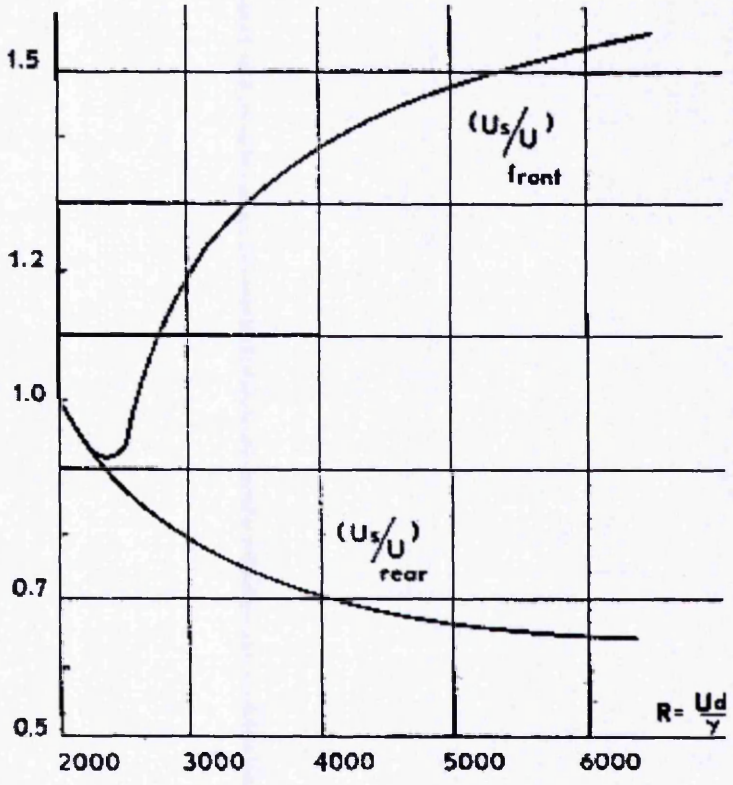

FIGURE 3.2. The results of Lindgren's (1969) (Lindgren 1969) experimental investigation of the speeds of the turbulent-laminar interfaces in turbulent patches.

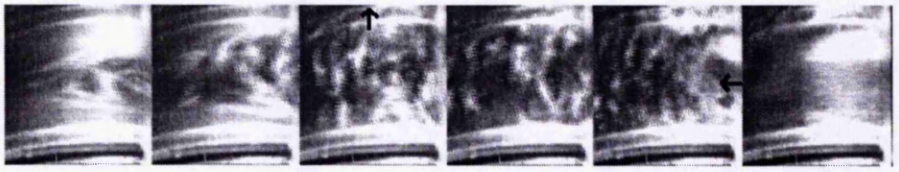

FIGURE 3.3. The image of a puff used in figure 2.9 but which additionally shows the reference locations used for measuring speeds

the front interface was found to be where the interface meets the wall of the tube. A typical image of a puff recorded at one location is shown in figure 3.3, the arrows indicate the positions of the reference points. Using this technique the speeds of the interfaces in twenty puffs were measured.

A graph of the average speed of the interfaces between the two reference locations plotted against the distance between them (puff size) is reproduced in figure 3.4. It can be seen from the figure that the puffs in the current experiment move at the mean flow velocity, in agreement with the observations of Lindgren (1969). As both of the interfaces are moving at the same speed the size of the puffs must remain the same. These results suggest that puffs at this Reynolds number are equilibrium puffs.

It is interesting also to note that while the most probable size of the puffs is eight pipe diameters the size of puffs varies considerably. However the speed of the interfaces (and hence the growth rate) do not depend on the size.

Using the fact that the puff is created at the disturbance generator when the disturbance was applied it is possible to calculate a second speed for the puff. This is the average speed of the puff from the disturbance generator to the first reference point. As the puff was not fully formed at this time is not possible to say when the front and back interfaces were at the disturbance generator. As an approximation we may say that front interface was at the disturbance generator when the disturbance was activated and the back interface was there when it is stopped. In figure 3.5 the average speed of the back interface each puff from the disturbance generator to the first observation point is plotted against the speed between the observation points. The fact that the points are all clus-

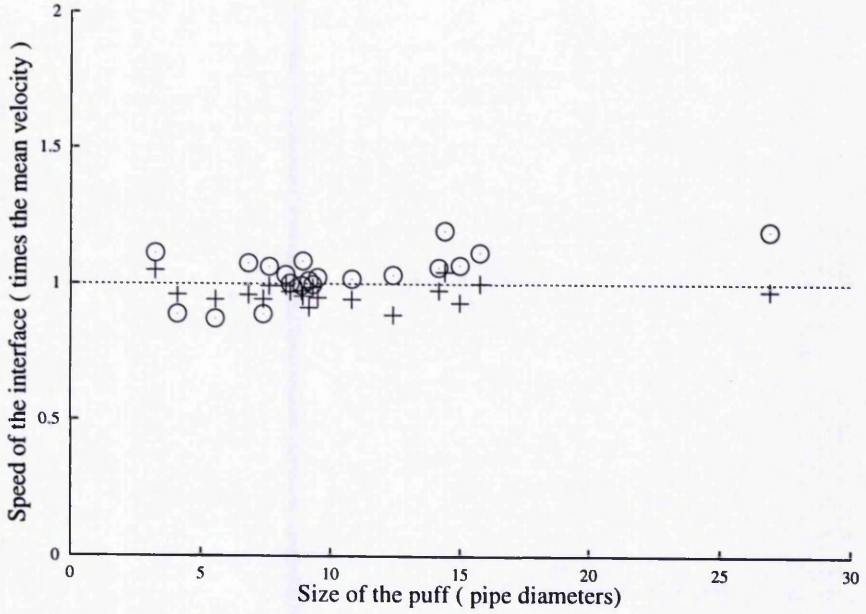

FIGURE 3.4. The circles represent the front interfaces while the crosses represent the back interfaces. The size of the crosses and circles is equal to the error on measuring the speeds. The measured speed has been made dimensionless by dividing it by the mean flow velocity and the size was non-dimensionalised by dividing by the diameter of the pipe.

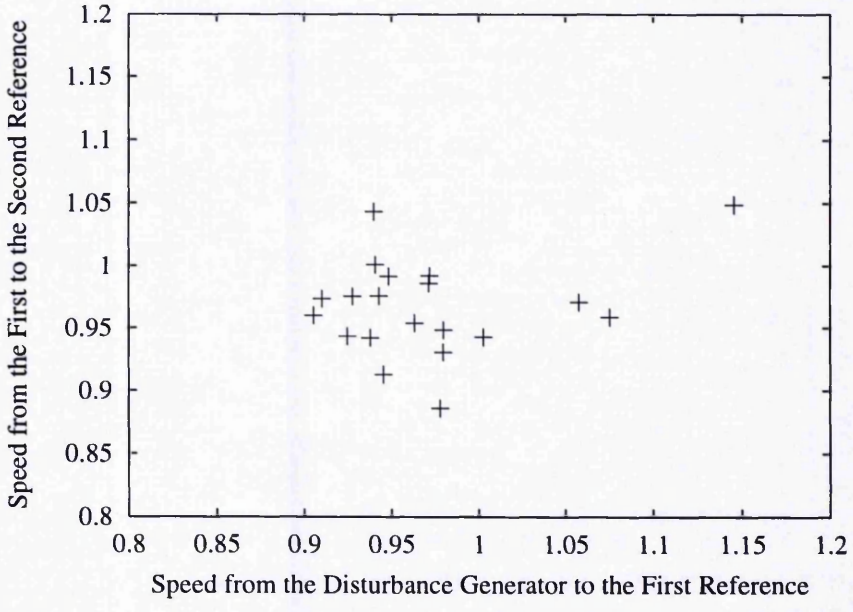

FIGURE 3.5. The average speeds of the back interfaces of puffs from 69 and 112 pipe diameters from the disturbance plotted against their average speed over the first 69 pipe diameters.

tered around the point $(0.95, 0.95)$ indicates that the speeds of the puffs are on average constant.

Chapter 4

Developing Pipe Flow Stability

This chapter begins with a discussion of existing knowledge of the form of the laminar entrance flow profile. A review of the published literature on the line linear stability of the entrance flow is presented together with a discussion of the associated neutral stability curve. Then measurements of the finite stability of entrance flow at Reynolds number 2170 are presented. The features of this stability curve are compared with those of the fully developed flow profile and linear stability.

4.1 The Developing Flow profile

Various methods of calculating the entrance flow profile were discussed in detail in section 1.3. Here the results of some of the different models are compared with each other and to available experimental data. Specifically, plots of the centre-line velocity of the flow against distance from the inlet are reproduced in figure 4.1. The difference between the measurements and predictions are at their greatest in the centre of the pipe. The centre-line velocity has been non-dimensionalised by dividing it by the mean speed. The distance from the inlet is non-dimensionalised by the diameter of the pipe and scaled by the Reynolds number. As noted in section 2.1 this scaling makes the results applicable to flows at different Reynolds numbers.

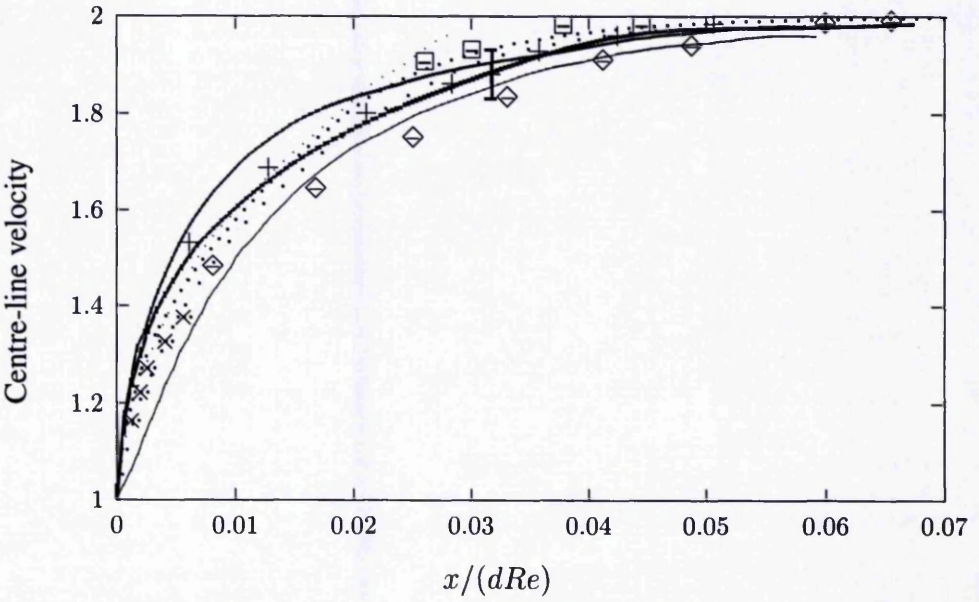

FIGURE 4.1. The data for this graph is largely taken from Fargie & Martin (1971) but with two later results have also been added. The experimental measurements are included as follows. Fargie & Martin (1971) $\diamond$, Reshotko (1958) $+$, Emery (1968)$\square$, Pfenninger (1952) $\times$, Darbyshire & Mullin (1995) (single errorbar), Nikuradse (1933)—. The calculated flow profiles are, Fargie & Martin (1971) $\cdots$, Boussinesq (1891) —, Schiller (1969) $\cdots$, Langhaar (1942) —, Mohanty & Asthana (1978) $\cdots$

The measurement from Darbyshire & Mullin (1995) was made in the same apparatus used in the current investigation. The 3 % error on this measurement arises from extrapolating the flow velocities measured at different locations to the pipe centre. All of the theoretical profiles agree with one another to within 8 %. The degree of agreement in the experimentally measured profiles is 6 %.

Reasons for the variation in the experimental results include the shape of the inlet and the background level of time dependent disturbances in the flow. The models all assume a sharp entrance where there is a 90^o angle between the pipe wall and the wall of the reservoir of fluid. Experimentally, it is found that at transitional Reynolds numbers this arrangement results in the formation of turbulent flow throughout the pipe. This is because the sharp edge introduces disturbances into the flow field due to separation of the boundary layer (Darbyshire & Mullin 1995). The solution is to make a smoothed pipe entrance such as the trumpeted shaped inlet used in our experiment. However, the shape of the entrance used was not the same in all of the experiments listed above.

Small deviations from the steady flow profile can have a significant effect upon the development of real flows. The momentum convection due to these perturbations can be comparable to the viscous momentum diffusion. Bandyopadhyay & Walton (1989) reported that unsteady flow with r.m.s amplitudes of 3 % - 5 % of the mean flow velocity reduced the entrance length by tens of percent. This is contrasted by the findings of Wygnanski & Champagne (1973) who found that disturbances of similar amplitudes *increased* the entrance length in their flow by > 10 %. It is not clear whether the apparent conflict in these results is due to the different Reynolds numbers used, differences in the apparatus or some other factor.

The flow profile that is assumed throughout the rest of this thesis is the one developed by Mohanty & Asthana (1978). This is a relatively recent model that uses an integral method (introduced in section 1.3). It was chosen because it contains all of the important features that are found in the experimental measurements of the developing flow.

In their calculation the developing flow is split up into two regions, the inlet region

and the filled region. In the inlet region the shear is assumed to be confined to a boundary layer near the wall of the pipe. At the pipe entrance the width of this layer is zero and the flow velocity is uniform across the cross section of the pipe. At locations downstream from the inlet viscous effects increase the size of the shear layer. The filled region starts when the thickness of this viscous layer has grown to one pipe radius. In both regions the rate of change of the radial velocity with distance down the pipe was assumed to be negligible. This simplifies the continuity and the Navier-Stokes equations to three linear equations. The flow profiles in both regions are assumed to be fourth order polynomials, substituting these into the Navier-stokes results in a pair of ordinary differential equations. These are solved numerically using a Runge-Kutta method.

Here the features of this calculated flow profile are examined with an emphasis on those features that are expected to effect the stability of the flow. A plot of the u-component of the fluid velocity is shown in figure 1.2. The flat velocity profile in the centre of the pipe is evident and is seen to decrease in size further from the inlet. The boundary between the two regions of flow is plotted in figure 4.2 as a function of scaled distance. It can be seen that the flat region of the velocity profile disappears at $x/(dRe) = 0.0182$. At this point the centre-line velocity is 88.8 % of the fully developed value. Near the walls the flow velocity varies as a fourth order polynomial that is zero at the wall and has zero gradient where it meets the inviscid core of the flow.

A plot of the acceleration of fluid elements in the flow is given in figure 4.3. The acceleration of a fluid element, $D\mathbf{u}/Dt$ is related to the velocity field by (from Acheson (1990) page 5)

$$\frac{D\mathbf{u}}{Dt} = \frac{\partial \mathbf{u}}{\partial t} + (\mathbf{u} \cdot \nabla)\,\mathbf{u}$$

For parallel flow which is steady in time this reduces to

$$\frac{Du}{Dt} = u\frac{\partial u}{\partial x}$$

The data published in Mohanty & Asthana (1978) was used to calculate u and its derivative was calculated from these values. The acceleration is greatest near the inlet where the

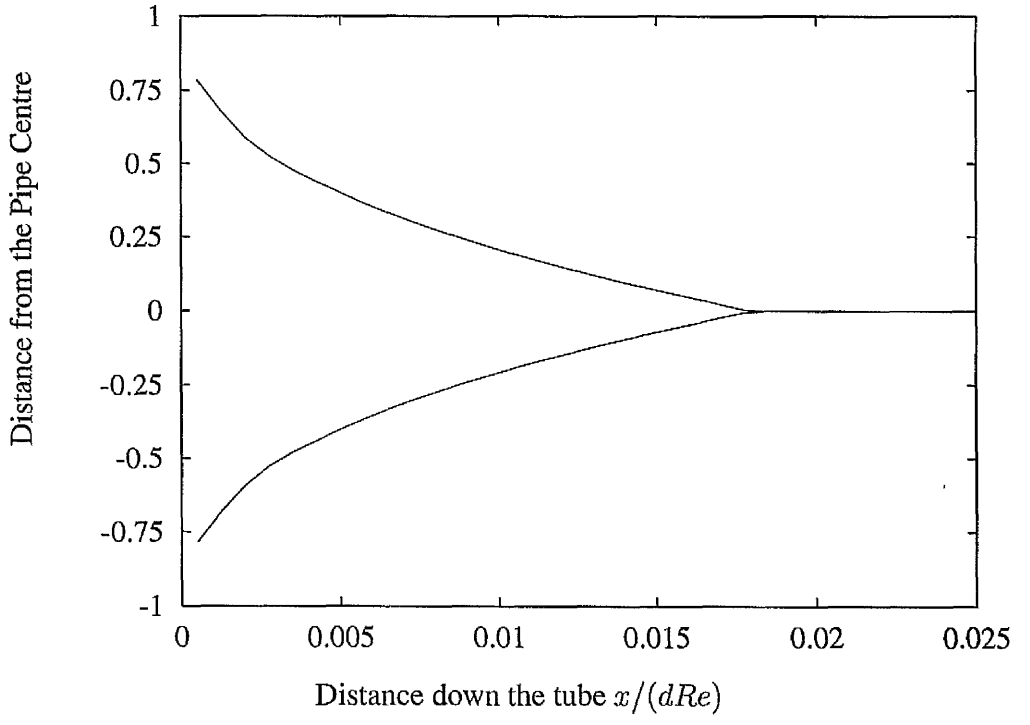

FIGURE 4.2. The boundaries of the viscous region and the central constant velocity core in developing pipe flow, according to the flow development theory in Mohanty & Asthana (1978)

flow profile differs the most from Poiseuille flow. As the flow becomes fully developed the acceleration drops to zero in all places. Close examination of figure 4.3 reveals a fluctuation in the acceleration at $x/(dRe) = 0.0182$ which is where inviscid core disappears. This corresponds to the location where the calculation switches between that for the inlet region and filled regions. At this point the coefficients that they calculated change rapidly to respond to the change. However the results of their calculation were tabulated with insufficient frequency, at this location, for the derivative to change smoothly. There are enough points to reproduce the velocity profile and this effect is not evident in figure 1.2. However the acceleration of the flow around $x/(dRe) = 0.0182$ cannot be deduced from the data with any accuracy.

It is commonly found that acceleration in a laminar flow has a stabilising effect upon the flow and that deceleration in flows makes the fluid flow less stable (Schlichting 1960). Where the flow is accelerating disturbances to the flow became stretched out and the flow is more stable. The deceleration of the flow near the walls is expected to make the outer part of the flow less stable than the core.

An important factor in the stability of a fluid flow is Rayleigh's inflection-point theorem. This states that a necessary condition for an inviscid flow to be linearly unstable is that there is a point of inflection in the flow profile (Drazin & Reid (1981) and references therein). The theory assumes parallel flow in plane geometry and the derivative is taken perpendicular to the flow direction. A point of inflection is a point at which the second derivative changes sign, this implies that the derivative is zero at that point. This stability analysis does not include the effects of viscosity which can have either a stabilising or destabilising effect upon the flow. Further the theorem does not guarantee that a flow profile will be unstable, it only states when an inviscid flow cannot be unstable. Despite all of these limitations it is found that in many flows, for which viscosity is important, that the formation of an inflection-point is associated with instability. For example it is noticed in boundary layers that a point of inflection in the flow is an important indicator of instability in the flow profile (Schlichting (1960) page 389). As discussed in the Intro-

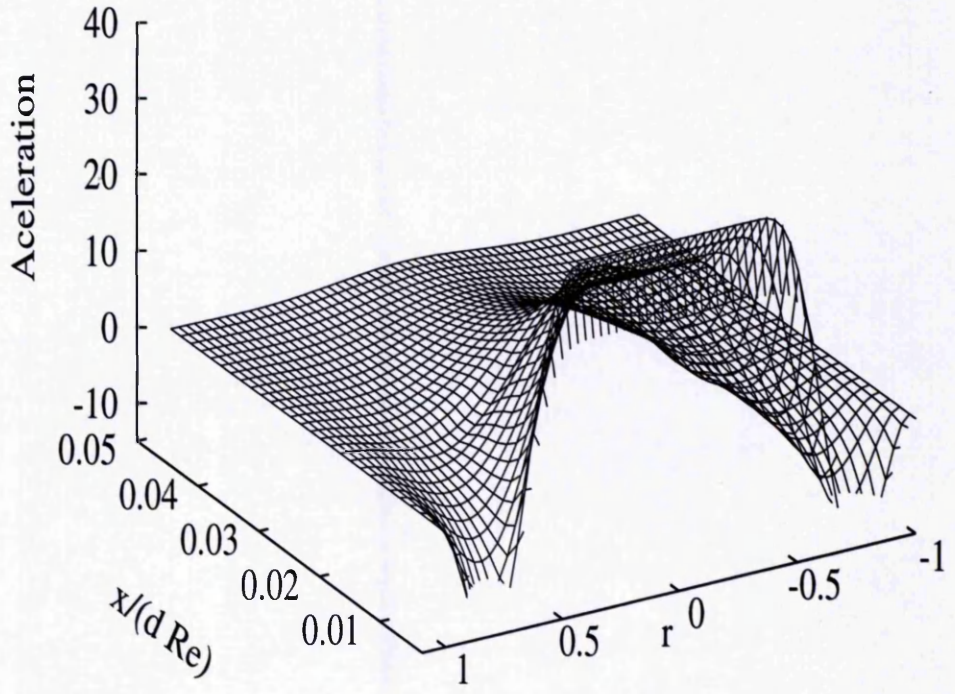

FIGURE 4.3. The acceleration of the flow in the downstream direction as a function of the cylindrical polar coordinates (r, θ, x). If Cartesian coordinates were used the net area under the graph would be zero as there is no net acceleration of fluid down the pipe.

duction shear flows that have points of inflection like jets and mixing layers have much lower critical Reynolds numbers for linear stability than those that do not. In pipe flow it was noted by Eliahou et al. (1998) that the transition to turbulence followed rapidly after transiently amplified perturbations formed a point of inflection in the flow profile.

There is a further stronger necessary condition for inviscid instability, called *Fjørtoft's theorem.* This assumes a parallel flow, $\mathbf{u} = u(r)$, of a fluid with negligible viscosity. A necessary condition for the flow to be linearly unstable is that

$$u''(u - u_i) < 0 \tag{4.1}$$

where u_i is the velocity at a point of inflection in the flow. In developing pipe flow the second derivative is everywhere less than or equal to zero. This theorem means that, in developing pipe flow, the point of inflection should not occur in the part of the flow with maximum flow velocity.

If the second derivative is very negative it would be expected that it would hard to produce a point of inflection in the flow. However, areas of the flow where the second derivative is not large and the velocity is not at its maximum may be weak points were the flow can be destabilised.

There have been linear stability studies of developing pipe flow that take into account the effects of viscous forces on the flow. These are the subject of the next section.

4.2 Linear Stability of Entrance Flow

The first theoretical investigation of the linear stability of developing pipe flow was performed by Tatsumi (1952) who carried out an analysis of the boundary layer formed the pipe entrance. Many theoretical investigations have been performed since, including Gupta & Garg (1981), Huang & Chen (1974), Garg & Gupta (1981) and D'Silva & Moss (1994), all using improved predictions of the shape of the developing flow. All of these investigators found critical Reynolds numbers above which the entrance flow became

unstable. Abbot & Moss (1993) found that the linear instability of the entrance flow disappeared at $x/dRe = 0.00819$ beyond which the flow is linearly stable all Reynolds numbers. The method behind calculating the linear stability was the same in outline for all of these studies and is as follows.

The base flow profile, $\mathbf{u}$, is calculated in cylindrical polar coordinates assuming parallel, axisymmetric flow i.e. $\mathbf{u}(r, \theta, x) = [u(r, x), 0, 0]$. The linear stability of the local flow profile is calculated at specified locations along the pipe. This is done by taking the flow profile at that point, $u(r, x = X)$, and filling a pipe with the profile such that $\mathbf{u}(r, \theta, x) = u(r)$ for all θ and x. The evolution of infinitesimal perturbations, that depend only upon θ and r, added on to the specified pipe flow are then calculated. If any perturbations grow then the flow is linearly unstable.

An implicit assumption of this analysis is that effects due to the flow profile changing with distance downstream are much less important than the shape of the flow profile. The reliability of this assumption is discussed later.

The neutral stability curve is the set of parameters for which the flow is just linearly stable i.e. one of the modes has a growth rate of zero. There are four parameters that govern the stability of the flow and so the neutral stability surface will in general be 4-dimensional. The parameters are the Reynolds number, the position in the flow at which the evolution was calculated and the wave numbers of the perturbation in the $\hat{\theta}$ and $\hat{\mathbf{r}}$ directions. Figure 4.4 contains a graph of a projection of this curve on to the Reynolds number, distance down the tube plane. Also included are the results of an experimental measurement by Sarpkaya (1975) discussed below. The critical Reynolds number for linear instability reduces to a minimum at some location downstream from the inlet. As the flow becomes fully developed the critical Reynolds number increases to high values, as expected from the linear stability of Poiseuille flow. The theoretical and experimental stability curves differ in the location of minimum stability and the lowest Reynolds number at which the flow becomes unstable.

The experiment of Sarpkaya was designed to test the linear stability results by in-

troducing small disturbances in the entrance flow. Three types of disturbance generator were used for this purpose. Two of these used wires that either moved in and out of the pipe or oscillated in the flow and cause a non-axisymmetric perturbation. The third disturbance generator was a sleeve positioned close to the tube wall which was rotated producing an axisymmetric disturbance. Each of these disturbance generators disturbed the flow continuously and the amplitude of the time dependent component of the flow was measured at different locations downstream. Poiseuille flow is time independent and so the amplitude of the time dependent flow features is a measure of the amplitude of the disturbance to the flow. When the disturbance decayed or grew slowly the amplitude was found to vary exponentially implying that the dynamics were indeed in the linear regime. Using this method the Reynolds number for no growth i.e. neutral stability, was found, for each perturbation type, as a function of the location at which the disturbance was added. It is this result that is plotted in figure 4.4. It was found that the disturbances always decayed in the fully developed flow and so the curve rises to to high Reynolds numbers at larger distances.

There are a number of differences in what is being measured in Sarpkaya's (1975) experiments and the linear stability analysis. The fact that the shape of the flow profile changes with downstream distance in the experiment but not in the analysis results in two important differences. In the analysis, the neglect of the streamwise velocity gradients would be expected to have an effect upon the growth rates. In the experiment, the growth rates were measured over some finite distance and so are average growth rates over the changing flow profile. The theoretical results are minimisations over different classes of perturbations. The experiment used only three types of perturbation, although the results from each perturbation type are similar.

As discussed in D'Silva & Moss (1994) these differences are unlikely to be the reason for the difference between the experimental and analytical results. This is because the models fail the most where the flow profile is changing at its slowest i.e. near the developed flow. There are two other differences that could cause the disagreement which

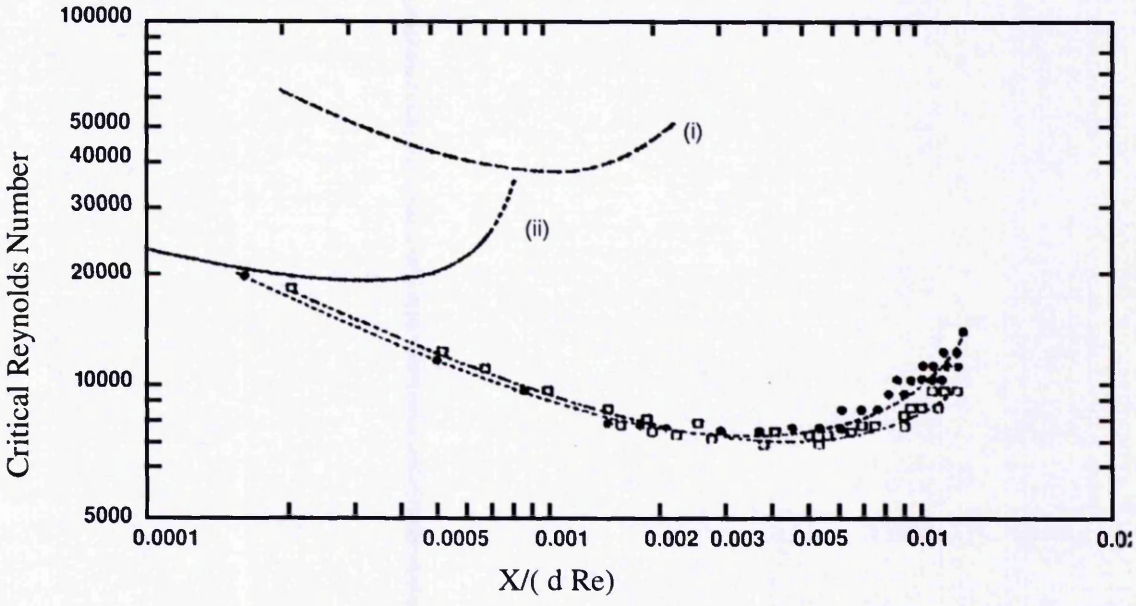

FIGURE 4.4. The Reynolds number at which infinitesimal perturbations have zero growth plotted against the location that the perturbation was applied. The theoretical predictions are i) Huang & Chen (1974) and ii) Tatsumi (1952). The experimental points are from Sarpkaya (1975). The filled circles are axisymmetric disturbances and the empty squares are non-axisymmetric.

were not discussed in D'Silva & Moss (1994). These are that the experiment uses finite, although small perturbations, which could lower the critical Reynolds number. The other difference is that in the experiment a number of different modes were present in the disturbance. This opens up the possibility of transient growth (Trefethen *et al.* 1993). As the level of perturbation was measured only over a finite distance the experiment may contain features of transient growth.

4.3 The Relationship between the Critical Disturbance Amplitude and Distance from the Inlet

The stability of the developing flow was measured by finding (at different distances from the inlet) the value of the critical disturbance amplitude, A_c. This was done for both types of disturbance generator at Reynolds number 2170. Graphs of A_c against the position where the disturbance was injected are shown in figure 4.5. The critical disturbance amplitudes were each calculated from the probabilities of transition at different disturbance amplitudes as explained in section 3.2. For example, the results of six-jet disturbance shown in figure 3.1 are included in this graph at 59.25 pipe diameters. The one-jet data in figure 3.1 are included for 113.2 pipe diameters from the inlet.

There are two features of the stability curves that are shared by the results of both types of perturbation. The value of A_c has its largest value close to the inlet and then decreases monotonically downstream levelling off to the fully developed value. However, the position that A_c starts to increase and its value far from the inlet are different for the two types of perturbation. The stability of the flow with respect to the six-jet disturbance increases substantially beyond $x/(dRe) = 0.014$. For the one-jet disturbance the increase is delayed until $x/(dRe) = 0.042$ and the rate of change of A_c with distance is lower.

The workings of the two disturbances were described in detail in section 2.2. It

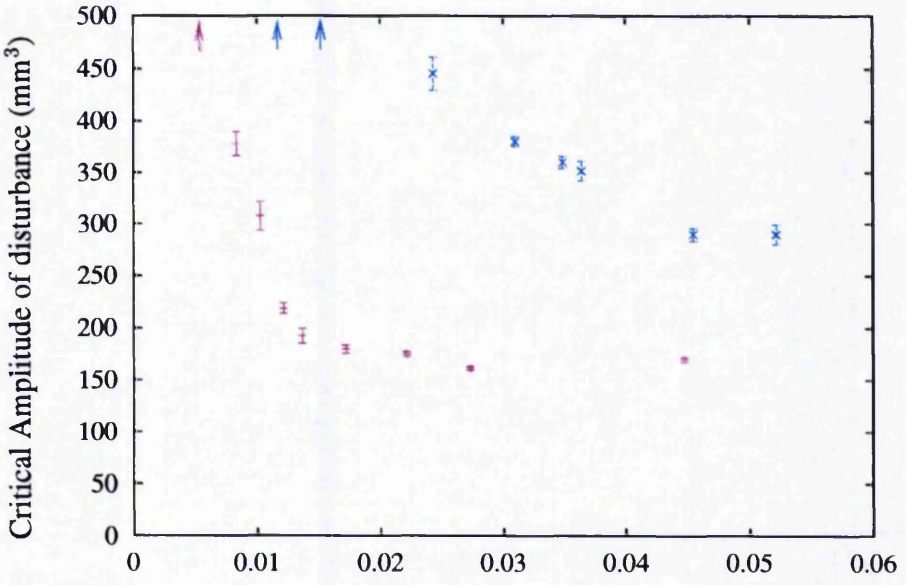

FIGURE 4.5. The variation of the critical disturbance amplitude with distance from the inlet for the two disturbance generators for Reynolds number 2170. The results for the six-jet injection disturbance are marked with horizontal crosses and the one-jet with diagonal ones. The arrows indicate that the critical disturbance amplitude is greater than 500.

was explained that the one-jet disturbance produces a single jet of fluid directed toward the centre of the flow. The six-jet disturbance generates six-jets of fluid equally spaced around the pipe. The line of injection is close to being tangential with the pipe wall. It is tangential to the extent that as the line crosses the pipe it is never more than 0.075 pipe diameters from the wall.

The critical amplitude approaches the fully developed value more quickly for the six-jet disturbance than the one-jet disturbance. This is likely to be due to the fact that the flow approaches the fully developed flow profile more rapidly near the pipe wall. This more rapid convergence to the fully developed flow profile is apparent in the extent of the inviscid core as well as the acceleration of the flow. The inviscid core of the developing flow retreats to the centre the of the pipe at locations further downstream from the inlet as discussed in relation to figure 4.2. The acceleration of the flow, as shown in figure 4.3, approaches zero more quickly in near the pipe wall. In the graphs in figures 4.6 a) and b) the finite-amplitude stability curve from figure 4.5 is re-plotted along with different characteristic properties of the laminar flow profile. In both graphs the quantities are plotted against scaled distance down the pipe. Examining how the different properties of the developing flow vary with distance is useful for determining which aspects of the developing flow determine its finite-amplitude stability. In figure 4.6 a) the finite-amplitude and linear stability curves are plotted together. The linear stability curve is from the experimental results obtained by Sarpkaya (1975), it is the mean of the critical Reynolds numbers from the axisymmetric and non-axisymmetric disturbances. Figure 4.6 b) contains a plot of the size of the central core of the flow for which the velocity gradient in the radial direction is precisely zero.

In comparing the finite-amplitude and linear stability curves in figure 4.6 a) it should be remembered that the measures of the stability are different in each case. The linear stability limit is measured in terms of the critical Reynolds number above which amplification of disturbances occurs. The finite-amplitude stability curve is the size of the perturbation required for the permanent breakdown of laminar flow. As the critical Reynolds

a)

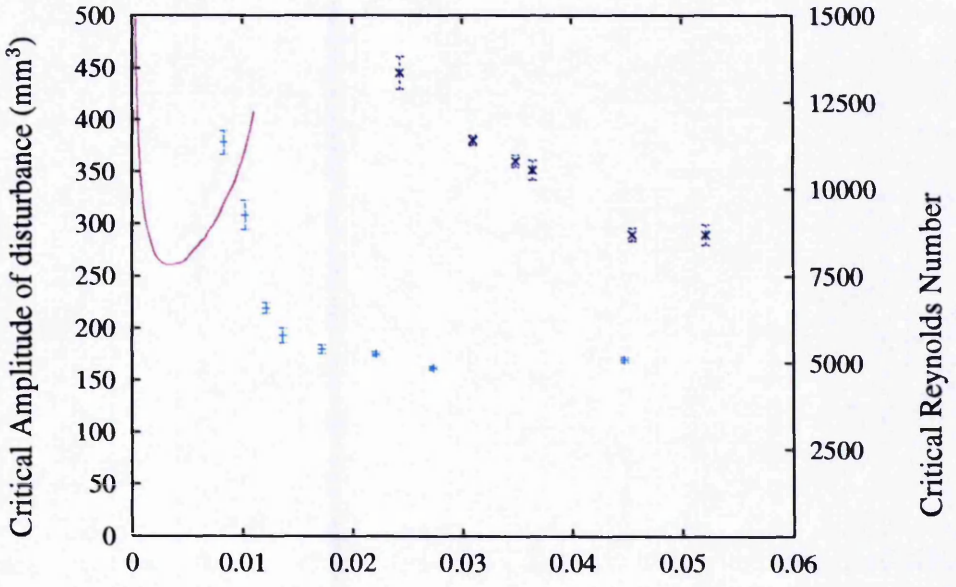

b)

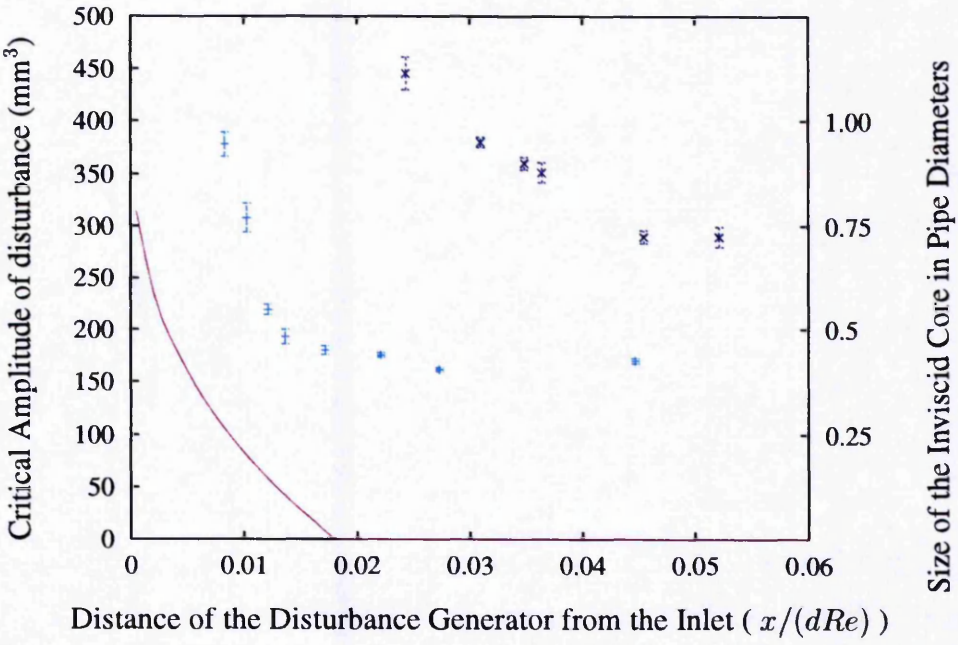

FIGURE 4.6. Graphs of the finite-amplitude stability of the entrance flow and different aspects of the developing profile against scaled distance from the inlet. In each graph the finite-amplitude stability results for the six-jet injection disturbance are marked with horizontal crosses and those for the one-jet with diagonal crosses, as in figure 4.5. The continuous lines represent a) The experimental neutral stability curve, from figure 4.4 and b) The size of the inviscid core of the flow, from figure 4.2.

number is the minimum value above which perturbations are amplified a greater value of the critical Reynolds number implies a more stable flow. Likewise a larger amplitude of the disturbance required to cause the break-down of laminar flow implies a more stable flow. This allows the linear and finite-amplitude stability curves to be compared. In comparing the two curves it is clear that the trends in the two types of stability are very different. The stability of the flow in the linear regime increases to large values beyond $x/(dRe) = 0.005$ while the finite-amplitude stability reduces monotonically levelling off between $x/(dRe) = 0.01$ and $x/(dRe) = 0.05$. Further the linear stability of the flow is only weakly dependent upon the type of perturbation used as may be seen from figure 4.4. However, at Reynolds number 2170 the type of perturbation used has a large effect upon the shape of the stability curve. The differences in the trend in the stability imply that the mechanism of transition in the entrance flow for finite-amplitude disturbances is very different from the linear process found at higher Reynolds numbers.

In figure 4.6 b) it may be seen that the width of the inviscid region of flow has shrunk to zero before the flow becomes unstable with respect to the one-jet disturbance. Hence the inviscid core of the flow plays no part in the transition to turbulence induced by the one-jet disturbance, over the range of disturbance amplitudes used. However, the value of A_c for the six-jet disturbance does change over the length of entrance flow in which the inviscid core shrinks. As the six-jet disturbance only perturbs the flow near the wall of the tube it seems unlikely that the central core has a large effect upon the stability. However, it is found that disturbances that are amplified fill the tube rapidly. For this reason it not possible to rule out the idea that the central core of the flow effects the stability of flow with respect to the six-jet disturbance.

The second derivative of the velocity profile and acceleration of the fluid are properties that depend upon the area of the flow under examination. In the following figures the acceleration has been non-dimensionalised by the mean velocity and the advective time. The advective time is the time taken for an object to travel one pipe diameter at the mean flow velocity. The velocity gradient is non-dimensionalised using the mean flow

velocity and the diameter of the pipe.

Figure 4.7 contains plots of the acceleration of the flow in the centre of the pipe and the finite-amplitude stability curve for the one-jet disturbance generator. Again a rapid change in the calculated velocity derivative appears at $x/(dRe) = 0.0182$ where the inlet and filled regions meet.

The acceleration is the only property of the developing flow that has been shown to change over the same region that A_c for the one-jet disturbance changes. The acceleration of fluid elements is expected to stabilise the flow. Hence the acceleration of fluid in the centre of the pipe is a good candidate to explain the stability of the flow with respect to the one-jet disturbance.

In figure 4.8 a) the six-jet finite-amplitude stability curve is plotted along with the local acceleration of the flow at 0.15 pipe radii from the pipe wall. This is at the maximum distance into the flow that the centres of the jets would reach if they travelled along the straight line that they were injected along. Figure 4.8 b) contains a plot of the second derivative of the flow profile at this location with scaled distance down the tube.

Both the deceleration of the flow and the variation of the second derivative may affect the flow's stability with respect to the six-jet disturbance. However, the deceleration of the fluid near the wall of the pipe would be expected to destabilise the flow in this region. The fact that the deceleration reduces with distance from the inlet cannot explain the reduction in the stability with distance. The deceleration is, however, likely to be an important factor in determining A_c for the six-jet disturbance in the developing flow.

The variation in the second derivative of the flow profile with distance from the inlet is capable of explaining the shape of the A_c curve. When u'' is small it is easier for a disturbance to create a point of inflection in the flow. This point of inflection could make the flow linearly unstable and initiate the transition to turbulence.

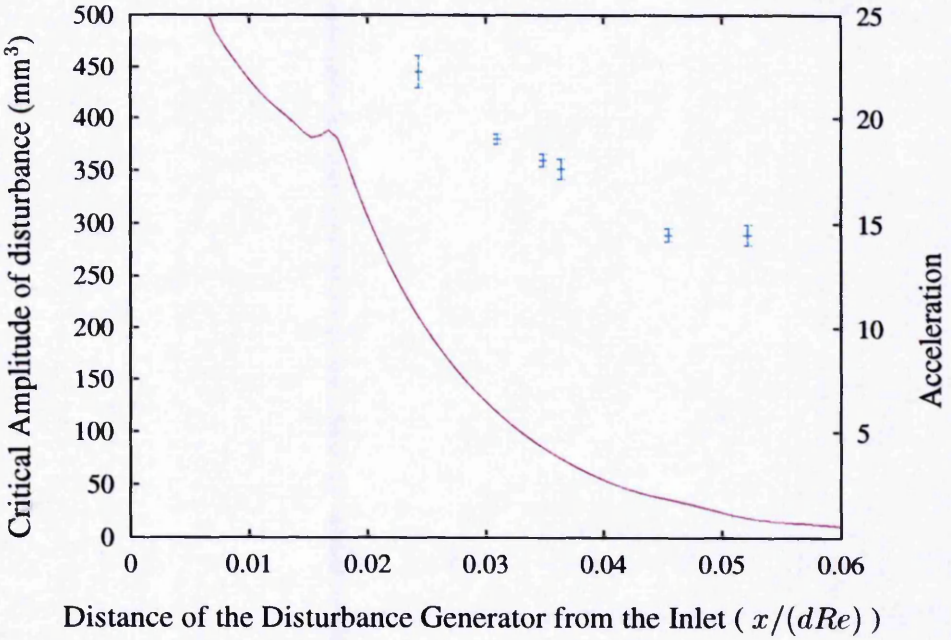

FIGURE 4.7. The value of A_c and the acceleration of the fluid along the centre of the pipe plotted against scaled distance from the inlet. The acceration was nondimensionalise by dividing it by the mean velocity squared and multipling by the pipe diameter.

a)

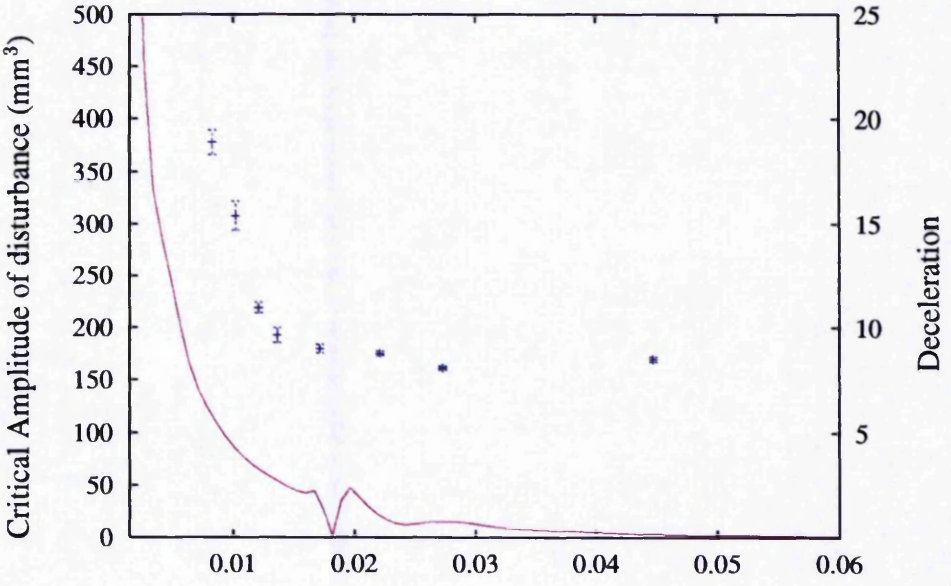

b)

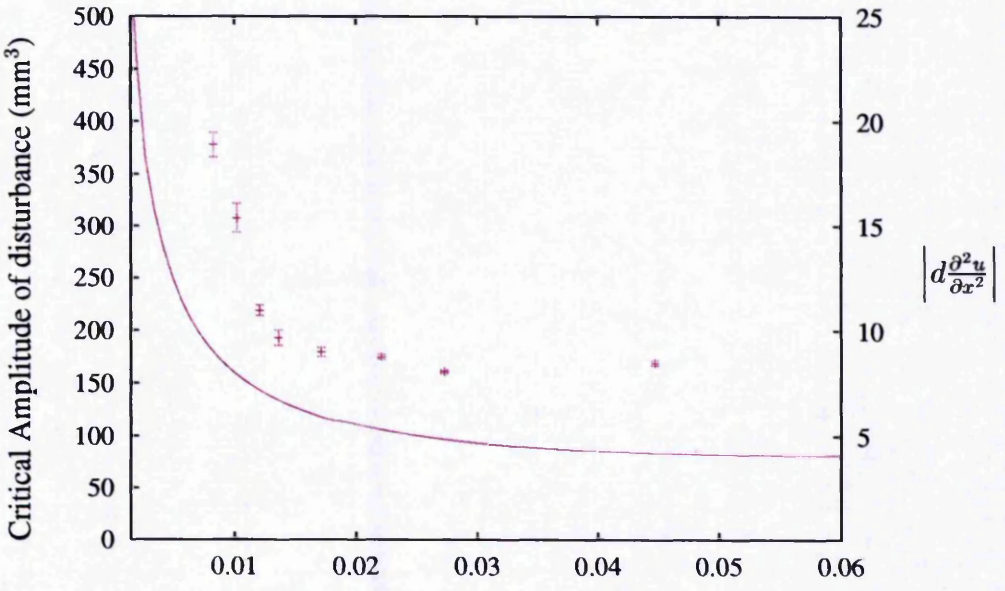

FIGURE 4.8. The value of A_c for the six-jet disturbance generator in entrance flow plotted with a) the acceleration (nondimensionalised as in figure 4.7) of the flow b) the modulus of the second derivative of the flow profile. In each case the properties of the flow are for 0.15 pipe radii from the wall.

Chapter 5

Entrance Flow Stability at Higher Reynolds numbers

In this chapter the results of the study the stability of the entrance flow are discussed for Reynolds numbers of three and four thousand. This chapter begins by comparing the transition to turbulence in fully developed pipe flow at these higher Reynolds numbers with that at Reynolds number equals 2170. Then the measurements of the relationship between the stability of the flow and the flow development at the higher Reynolds numbers are presented. These results are compared to the entrance flow stability results for Reynolds number 2170 which were discussed in the last chapter. They are also compared with the stability measurements of Sarpkaya (1975) which were performed on entrance flow at Reynolds numbers of 7000 and greater. Then the average shape of the probability versus disturbance amplitude relationship is calculated by combining the probability measurements for different parameters. Correlations between the parameters and the shape of the curve are sought.

Re	Distance from Disturbance			
	0	22.7	57.7	102.7
2170	1	0.9 ± 0.2	0 ± 0.05	0
3000	1	0.54 ± 0.15	0 ± 0.08	0
4000	1	0.2 ± 0.3	0 ± 0.09	0

Table 5.1. The probability that a puff produced by the disturbance generator and decayed downstream had not relaminarised at different distances. The probability of a puff being observed 107 pipe diameters from the disturbance generator is necessarily zero.

5.1 Measuring the Critical Disturbance Amplitude

Before it is possible to measure the probability of sustained transition, the lifetimes of transients must be measured. To this end the investigation outlined in section 3.3 was repeated at Reynolds numbers of 3000 and 4000.

The proportion of transients that persist to different distances from the disturbance generator are listed in table 5.1. The first row is for Reynolds number 2170 and is taken from table 3.2 for comparison. The table is the result of approximately 500 experimental runs and the errors were calculated for each probability from the number of runs as explained in 3.2. It can be seen that as the Reynolds number increases transients persist over shorter distances down the pipe. As the flow rate is directly proportional to Re, the lifetimes of the transients must therefore reduce rapidly with increasing Re.

The disturbance generator was 67.2 pipe diameters from the inlet in all three investigations. At Reynolds numbers of 2170, 3000 and 4000 the maximum flow velocity is, respectively, 85 %, 81 % and 77 % of that of fully developed flow at this location. The differing levels of development of the flow at each Reynolds number can be expected to have an effect on the development lengths of puffs. However, the percentage change in the development of the flow is small compared with the variation in the lifetimes of the transients. Hence, it may be concluded that the development lengths of turbulent puffs in fully developed flow decrease as the Reynolds number is increased.

This trend is in agreement with the observations of Darbyshire & Mullin (1995) who found that the decay length of transients were much greater at $Re = 1800$ than $Re \approx 2200$. There is further supporting evidence for this conclusion from the numerical simulations of Shan et al. (1998). They simulated the transition to turbulence in pipe flow and found that the time taken for the flow to reach its final state scales as Re^{-1}. This is in accordance with the results presented in table 5.1.

In section 3.3 it was found that a distance of 58 pipe diameters is sufficient for the decay of transients at Reynolds number 2170. At these higher Reynolds numbers it would be possible to observe the flow closer than 85 pipe diameters from the disturbance. However, in this investigation it was never necessary to use the disturbance closer than 74.8 pipe diameters from the observation point.

Figure 5.1 contains a graph of the probability of transition against disturbance amplitude for Reynolds numbers 2170, 3000 and 4000. The experiments were performed using the six-jet disturbance generator when all parts of the flow profile were within 95% of the fully developed flow profile. The probabilities were measured by repeating the experiment at the same disturbance amplitude and calculating the ratio of number of transitions to the total number of runs. Each point on the graph contains approximately 15 runs to give an error of 0.1 on the probability. It may be seen that the relationship between the probability of transition and the amplitude of disturbance is qualitatively the same at all three Reynolds numbers. The probability of transition is zero for disturbances below a certain amplitude. Above that threshold amplitude, the probability increases approximately linearly until the probability reaches one. The changes that occur as the Reynolds number is increased are that the disturbance amplitude for which the probability is 0.5 decreases. The probabilistic width, W,which is the difference between the disturbance amplitudes for which the probability equals zero and one is 36 at 2170. At higher Reynolds numbers this decreases to 18 at Reynolds number 4000.

The values of A_c at the three different Reynolds numbers, for both types of disturbance generator all in the fully developed flow are plotted in figure 5.2. Three lines

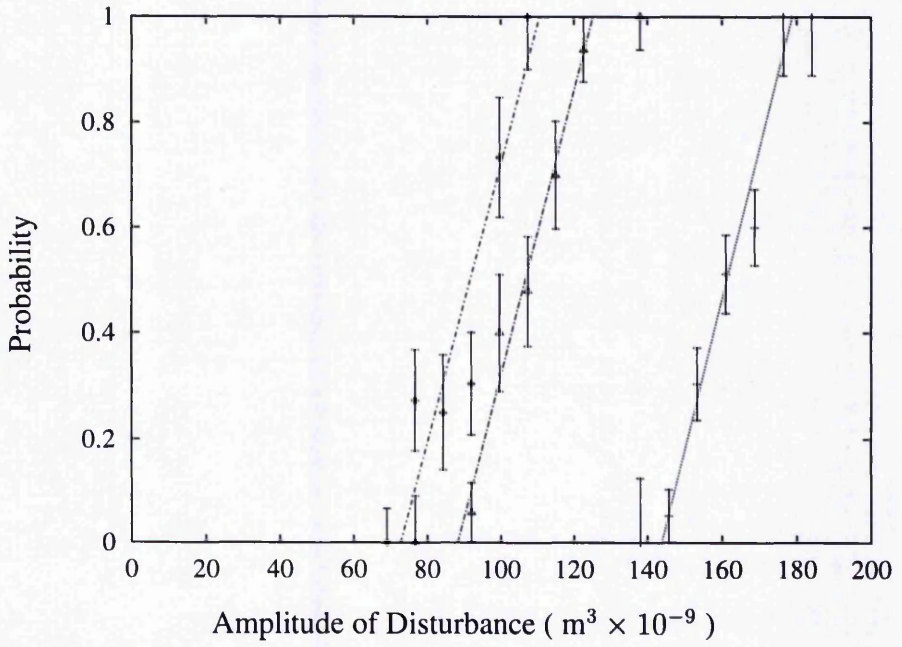

FIGURE 5.1. The probabilities of transition at Reynolds numbers of 2170, 3000 and 4000 are plotted using crosses, open triangles and filled diamonds respectively.

Disturbance Generator	Parameters		
	Re_c	γ	d
Six-jet	2070 ± 80	0.21 ± 0.06	500 ± 200
One-jet	2080 ± 40	0.51 ± 0.07	3000 ± 1800

Table 5.2. The values of Γ, Re_c and d for the fully developed flow.

plotted in this graph are the measurements from Darbyshire & Mullin (1995). The results are for three different designs of disturbance generator each used a common measure of disturbance amplitude. The behaviour that is common to to all of the types of perturbation is that the disturbance amplitude increases to large values below $Re = 2000$ and levels out high Reynolds numbers. These results are consistent with the critical amplitudes varying in accordance with equation 1.4 critical Reynolds number and the rate of flattening depend in general upon the type of disturbance as predicted by Dauchot & Daviaud (1995).

The points from the current investigation have been fitted to equation 1.4. There are three data points for each type of disturbance. However, there are also three fit parameters in the fit equation. This means that the fit is exact for data set but the errors on the parameters are large. The values of the parameters, Γ, Re_c and the constant of proportionality, d, are given in table 5.2. The errors on Γ, Re_c and d cannot be calculated from the goodness of the fit. Instead the errors were estimated by observing how the fit parameters changed as the data points were varied inside the error bars. These errors assume that equation 1.4 is valid over the range of Reynolds numbers used, more measurements would be required to confirm this, however. The values of Re_c and γ are relatively insensitive to changes in the critical disturbance amplitudes and so can be estimated with reasonable accuracy. The value of d changes a great deal and so is more uncertain.

In figure 5.3 the probabilistic widths for the fully developed flow is plotted against the Reynolds number of the flow. The probabilistic width have been scaled by the value of A_c in each case so that it is dimensionless. It is clear that, to within the errors, the size of the scaled probabilistic width for the one-jet disturbance is independent of the

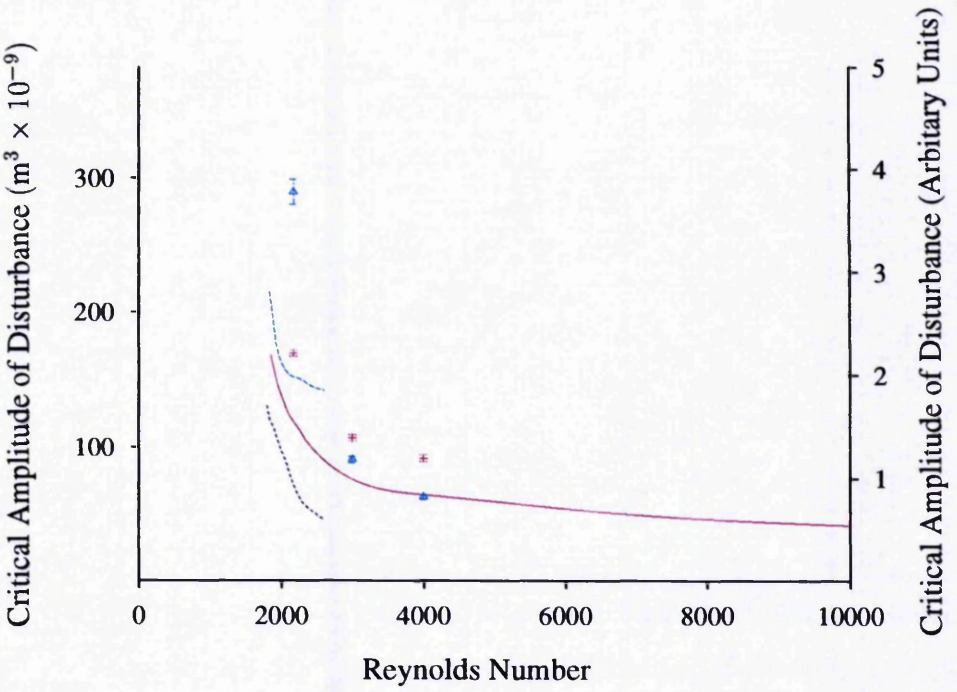

FIGURE 5.2. The variation of the critical amplitude of disturbance fully developed flow with Reynolds number. The one-jet disturbance generator △, six-jet + and the results of Darbyshire & Mullin (1995), push-pull (dotted blue), single-jet (dotted green) and six-jet (solid red).

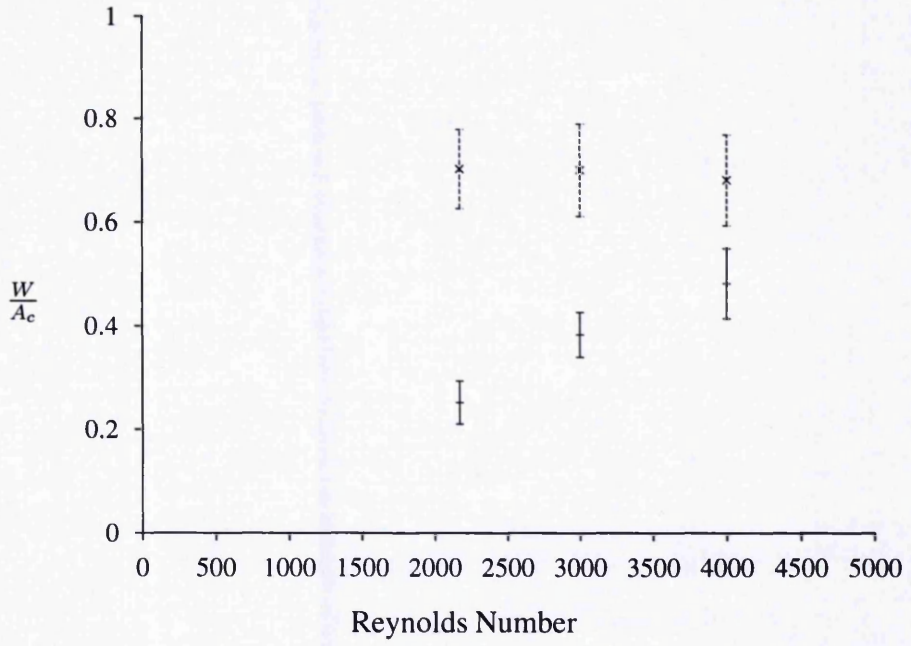

FIGURE 5.3. The variation of the critical amplitude of disturbance in fully developed flow with Reynolds number. The measurements for the six-jet disturbance are marked with + and the one-jet disturbance with ×.

Reynolds number. For the six-jet disturbance the measured values of W/A_c increase with Reynolds number. Because of the size of the errors it is not possible to predict whether the two reach the same value. There is another factor that W depends upon and this is discussed later in this chapter.

The velocities in the pipe flow are proportional to the Reynolds number. As the velocity at which fluid is pumped into the flow from the disturbance generators does not increase with Reynolds number it is reasonable to ask whether the jet from the one-jet disturbance generator still reaches the centre of the flow at higher flow rates.

To check the progress of the jet into the flow the water that supplies the one-jet disturbance was replaced by ink. The pattern of injected ink was then captured using a camera. Images of the distribution of ink are shown in figures 5.4 a), b) and c). Fluid in the pipe flow is moving from right to left in the diagrams and the pictures were taken shortly after the disturbance generator was activated. The disturbance amplitude in each case was the

critical disturbance amplitude at that Reynolds number. At the higher Reynolds numbers it can be seen that the ink has spread further downstream at the time the picture was taken due to the increased flow speed. This spreading out makes the ink less visible at higher Reynolds numbers, however, the ink always reached the centre of the pipe.

There are a great number of similarities between the transition to turbulence at Reynolds numbers of 3000, 4000 and 2170. Disturbing the flow still results in a probability of transition to turbulence and the critical disturbance amplitude can be calculated in the same way as it was at $Re = 2170$. The one-jet disturbance disturbs the flow in the middle of the pipe at all three Reynolds numbers. These similarities allow the investigation that was the subject of the last chapter to be extended to higher Reynolds numbers. This is the subject of the next section.

5.2 The Variation of the Critical Disturbance Amplitude with Development of the Flow

The critical disturbance amplitude was measured at different locations down the pipe at Reynolds numbers of 3000 and 4000. These results are plotted along with the $Re = 2170$ results for the six and one-jet disturbance generators in figures 5.5 a) and b) respectively. In both graphs distance from the inlet has been scaled so that the shape of the undisturbed flow profile is the same for the different Reynolds numbers. Two main features of the change in the stability of the entrance flow with scaled distance were common to both disturbance generators at each Reynolds number. These were that the amplitude of disturbance required for transition was greatest near to the inlet and that it levels off to a constant value at large distances. The changes that occurred as the Reynolds number was increased were that A_c was reduced and approached its fully developed value more quickly. The curves for both disturbance generators also approached the same shape for higher Reynolds numbers.

a)

b)

c)

FIGURE 5.4. Images of the one-jet disturbance generator shortly after it was activated at different Reynolds numbers. Here ink has replaced the water that is normally injected into the flow so that the resting place of the injected fluid can be made out. Arrows have been included to aid the eye to the areas of ink.

a)

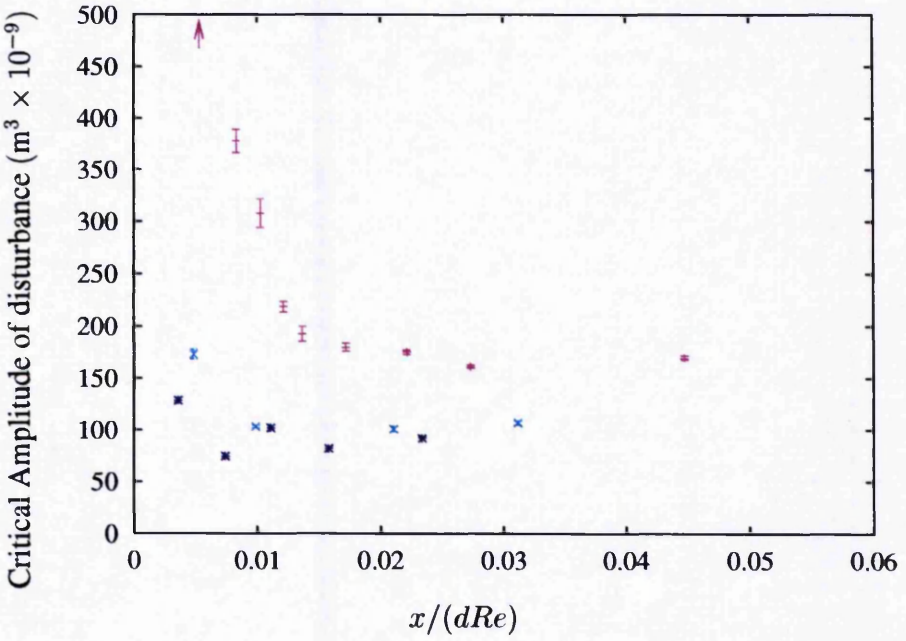

b)

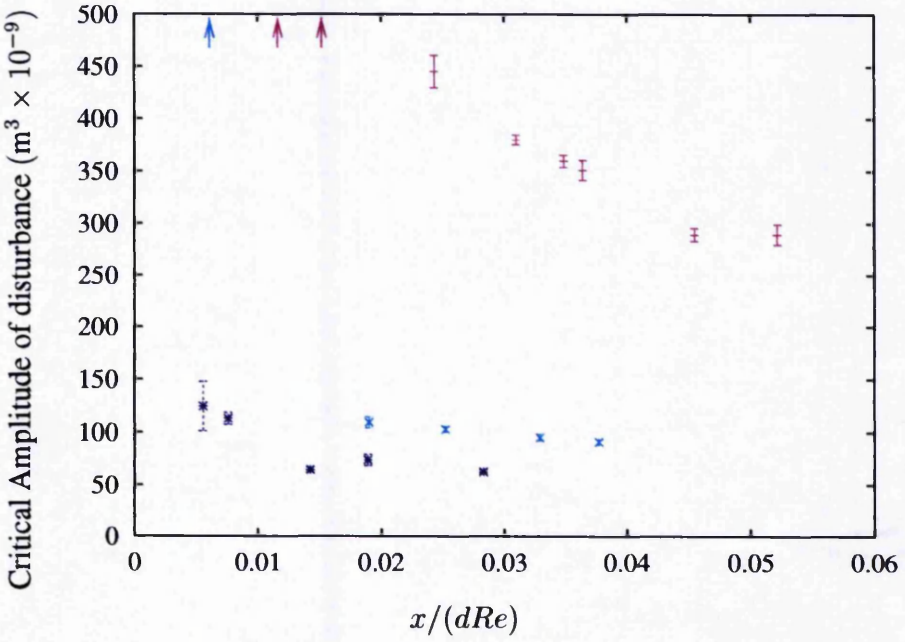

FIGURE 5.5. The critical amplitude of disturbance for pipe flow disturbed at different scaled distances from the inlet for a) the six-jet disturbance b) the one-jet disturbance. In each graph the Reynolds number equals 2170 results are plotted using +, for $Re = 3000$ × and 4000 ⋆.

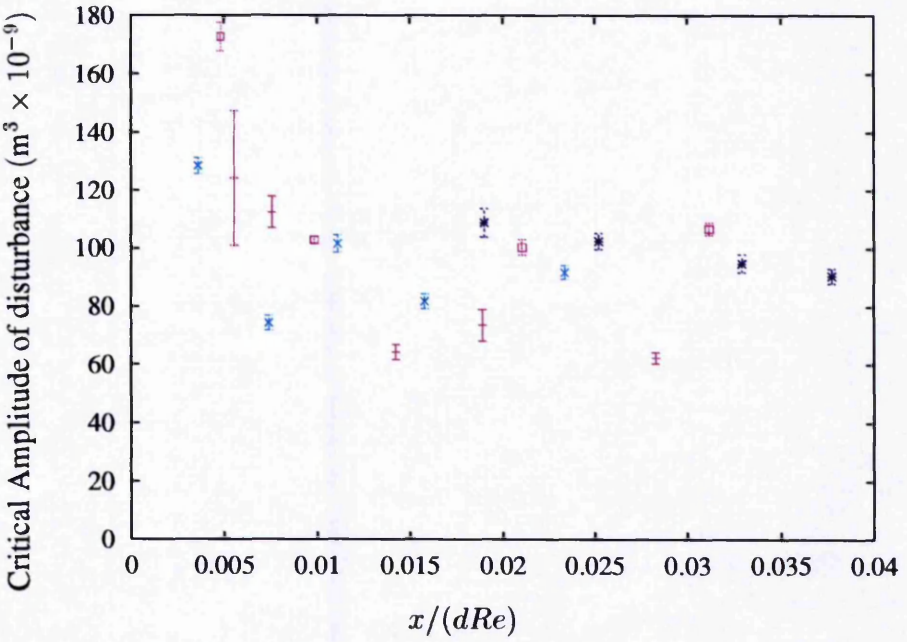

FIGURE 5.6. The critical amplitude of disturbance for pipe flow disturbed at different scaled distances from the inlet. For $Re = 3000$ $*$ is used for the one-jet disturbance and $\square$ for the six-jet. At $Re = 4000$ one-jet $(+)$ and six-jet $(\times)$.

The $Re = 3000$ and $Re = 4000$ results for both disturbance generators are plotted again in figure 5.6. The values of A_c are greater for the $Re = 3000$ than 4000. The main difference between the trends for the different disturbance generators is the distance from the inlet at which A_c increases. At all three Reynolds numbers it is the stability of the flow with respect to the six-jet disturbance that levels off to a constant value closer to the inlet.

A feature of the $Re = 4000$ data is that the scatter is greater than would be expected by the error bars. This is not true for either the $Re = 2170$ or the $Re = 3000$ data. Small differences in the conditions in the pipe due to re-assembling and cleaning the apparatus were found to change the ratio of the number transitions to the total number of runs. As a result the real errors on the $Re = 4000$ measurements are greater than that indicated by the error bars which only include the sampling error.

In order for the apparatus to be used at higher Reynolds numbers more control would be needed over external perturbations. For example a reduction in ambient vibration levels and increased settling times between runs of the experiment.

It is clear from the change in the relationship between A_c and distance from the inlet (figure 5.5) that the stability of the flow does not relate to the shape of the developing flow profile at $Re = 3000$ and $Re = 4000$ in the same way as it did at $Re = 2170$. Also at higher Reynolds numbers the type of disturbance used becomes less important in determining the value of A_c. There is one trend in the changing pattern of stability that may explain the shape of the stability curve at higher Reynolds numbers. This is the fact that the shape of the finite-amplitude stability curve appears to converge with that of the linear neutral stability curve as the Reynolds number is increased. Before the similarities of the finite and linear neutral stability curves are discussed the examination of the results will be completed by reporting on the variation the probabilistic widths.

Figure 5.7 contains graphs of the probabilistic width, W, and also A_c against distance from the inlet. There are three graphs for six and one-jet disturbance generators, one for each Reynolds number. The variation of the probabilistic widths with Reynolds number

for both types of disturbance in fully developed flow was plotted in figure 5.3. The probabilistic widths increase from their fully developed values when A_c becomes large close to the inlet.

The probabilistic widths do not necessarily increase near the inlet, however. This is shown in figure 5.7 e), which is for six-jet disturbance at $Re = 4000$. At these parameters W stays small even close to the inlet principally because A_c remains small.

Close examination of figure 5.7 a) reveals that W is not directly related to the gradient of A_c either. This is because W does not become large when A_c begins to increase and therefore has a large gradient. All that can be said is that, for each disturbance type and at each Reynolds number, the probabilistic width increases when ever A_c increases.

5.3 Comparison of the Stability of Entrance Flow in the Linearly Stable and Unstable Regimes

The experiments of Sarpkaya (1975) were performed at Reynolds number 7000 and above. Sarapkaya measured the critical Reynolds number above which perturbations are amplified, a higher critical Reynolds number implies a more stable flow. A higher value for the critical disturbance amplitude in the current experiment also implies a more stable flow. Hence, it might be expected that as the Reynolds number used in the current experiment is increased, toward 7000, the shape of the stability curve would approach that measured by Sarpkaya. Sarpkaya's experimental measurements and some theoretical linear stability predictions were plotted in figure 4.4.

For both types of disturbance generators used in the current investigation, the critical amplitude approaches a constant level more quickly as the Reynolds number is increased. The finite-amplitude stability does not reach a minimum, as the neutral stability curves do. However, the point at which A_c begins to change rapidly can be made out. In figures 5.8 a) and b) the finite-amplitude stability curves for the two different disturbance types

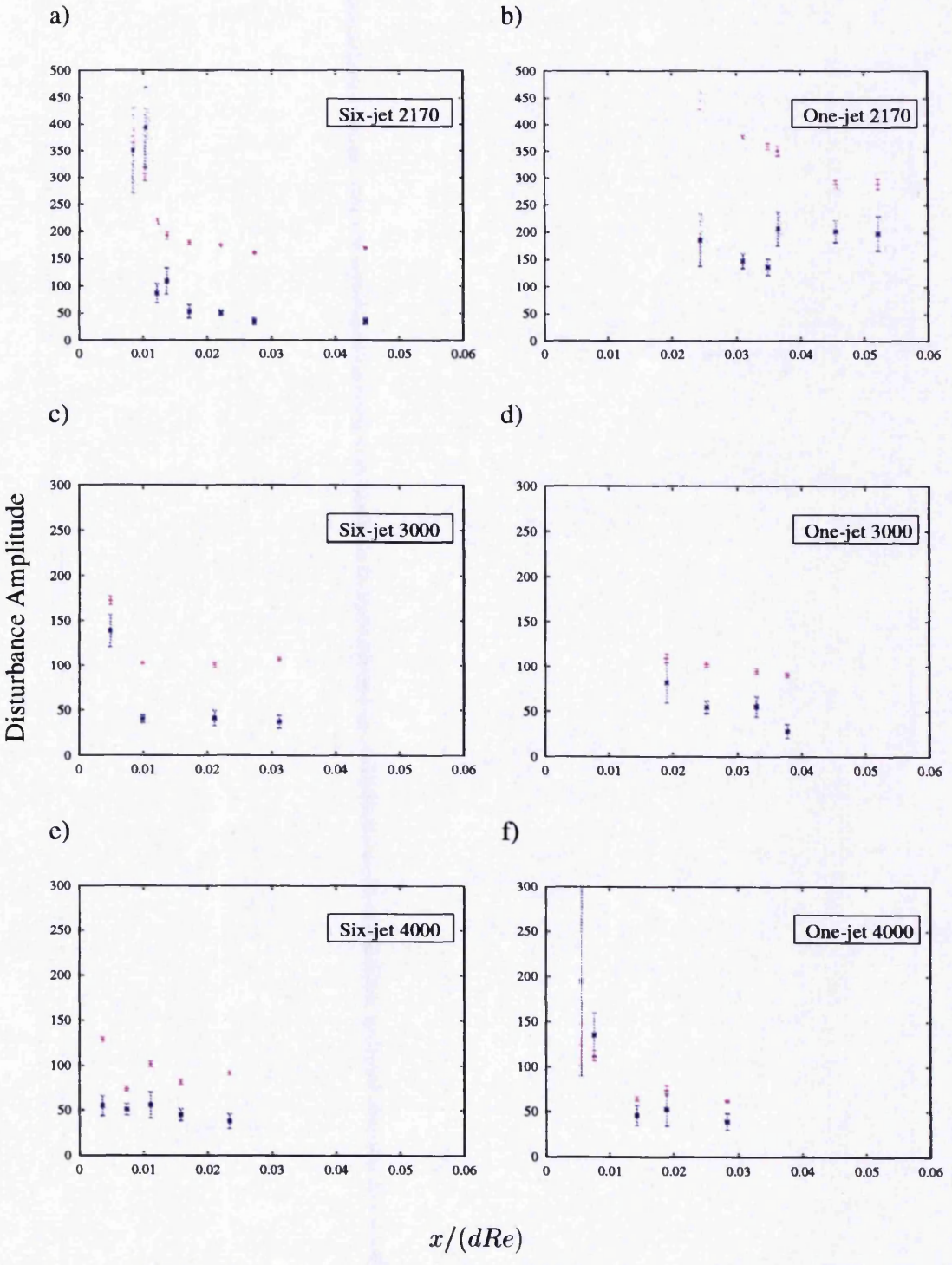

FIGURE 5.7. Graphs of the probabilistic width (blue stars) and the critical disturbance amplitude (purple crosses) against distance from the inlet. The graphs are plotted for each disturbance generator at different Reynolds numbers.

are re-plotted with the neutral stability curve measured by Sarpkaya. As the Reynolds number is increased the point at which A_c stops decreasing rapidly and gradient approaches zero occurs closer to the inlet. It is consistent with this point occurring at the same place as the minimum in the linear neutral stability curve at Reynolds number 7000.

Increasing the Reynolds number does not change the monotonically decreasing nature of the stability relationship, however, over the range of Reynolds numbers investigated. This feature of the shape of the finite-amplitude stability curve does not appear to converge smoothly toward that of linear neutral stability. It is likely that the critical disturbance amplitude remains greater in the entrance flow than the fully developed flow until the developing flow becomes linearly unstable. The amplitude of disturbance required to cause transition in the linearly unstable region of the flow maybe quite small. This sudden drop in the critical disturbance amplitude destroys the monotonically decreasing shape of the stability curve. It would be interesting to extend the experiment to Reynolds numbers of up to 10000 where some parts of the flow are believed to be linearly unstable and others stable.

5.4 The Shape of the Probability function

In section 3.1 the method of approximating the probability distribution by three straight-lines was introduced. There is one line at probability zero, one over the probabilistic region and another at probability equals one. Here the results of many data sets are combined to find the shape of the probability distribution more accurately. To do this it is useful to scale the amplitudes used in the plots so that the scaled probabilistic width and critical disturbance amplitude are the same for all of the plots. The chosen scaled amplitude, A^* has the formula

$$A^* = \frac{A - A_c}{W} \tag{5.1}$$

The critical disturbance amplitude is zero in this scaled quantity and the probabilistic width is equal to one. Graphs of the probability of transition against A^* will lie on top of

a)

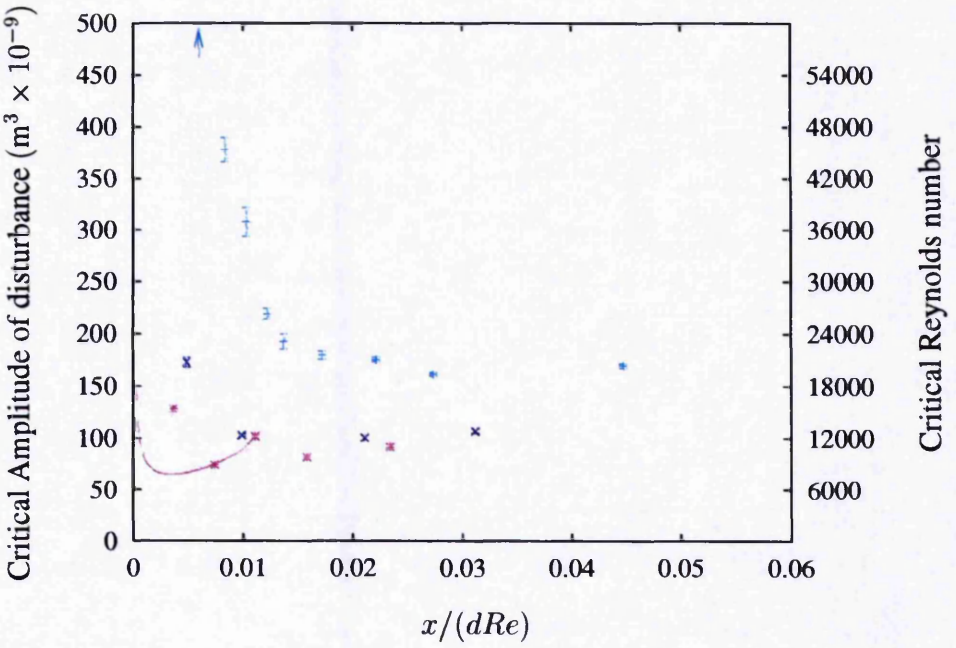

b)

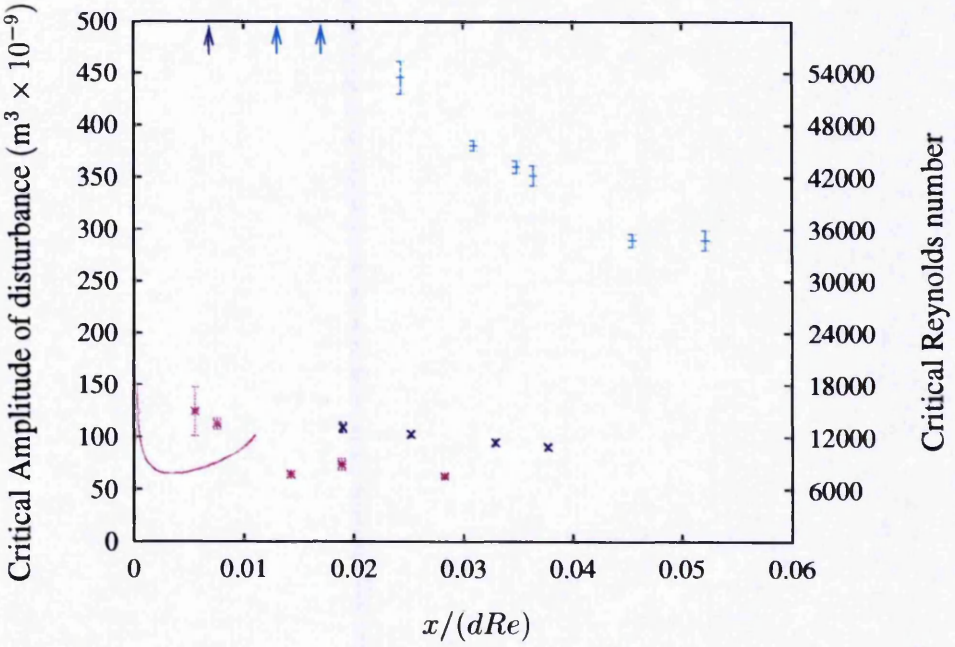

FIGURE 5.8. Graphs of the linear neutral stability curve and finite-amplitude stability curves for a) the six-jet disturbance and b) the one-jet disturbance. The solid line is the linear neutral stability curve, the green points are the finite-amplitude stability at Reynolds number 2170, the blue ones for $Re = 3000$ and $Re = 4000$ is in pink.

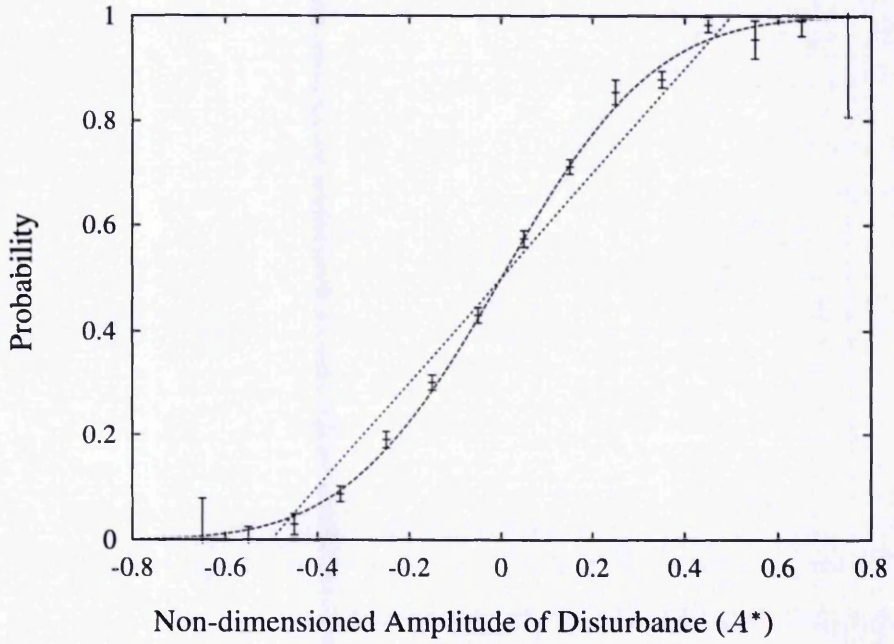

FIGURE 5.9. The average probability of transition from all of the data sets against scaled amplitude.

one another, if the shape of probability versus amplitude curve is the same. Equation 3.1 for the line of best fit over the probabilistic region is transformed to

$$p = A^* + 0.5 \qquad \text{intermediate } A \tag{5.2}$$

The result of averaging all of the data sets produced throughout this investigation are shown in figure 5.9. There were 32 individual data sets with a total of 5797 runs. The probabilities have been combined into 20 bins between $A^* = -1$ and $A^* = 1$. An error function of the form $0.5 + 0.5erf(eA^*)$ has been fitted to the data. The only fit parameter is e the value of which was found to be 2.67. The equation of the line of best fit of this combined data set is given accurately by equation 5.2 and is included in the graph for comparison. If the gradient of the error function at $A^* = 0$ was the same as the line of best fit e would be equal to two. The value of e is greater than two because of the tails of the error function.

Both the straight line fitting function and the error function are symmetric and cross

at the point $(A = A_c, p = 0.5)$. This means that A_c is little affected by the choice of fitting function. The reason a straight line was fitted to the data is because the error function is not linear. When the error function is fitted to data the resulting fit parameters can vary depending upon initial values of the parameters used. Also the nonlinear fit does not always converge without a good guess at the final fit parameters.

To see if the flow parameters affect the shape of the probability curve, graphs were made by combining data sets with one common parameter. For example, data sets from runs at the same Reynolds number were normalised and combined as above. Also data sets for both types of disturbance generator and those for fully and undeveloped flow were combined separately. It was found while the size of the probabilistic region depended upon all of those parameters, the shape of the relationship between probability and amplitude did not.

An example of this is shown in figures 5.10 a), b) and c) which contain graphs of the average probability at the three different Reynolds numbers. The graphs were made by averaging data sets from when the flow was disturbed at different degrees of development and with the two disturbance generators. The graphs for Reynolds numbers of 2170, 3000 and 4000 are the result of averaging 14, 8 and 10 data sets, or 3126, 1258 and 1413 experimental runs respectively. These results were combined into 20 bins. The error function that is included in each graph is the same error function that was fitted to the average of all the data sets in figure 5.9. It can be seen that the error bars are larger in these graphs than they were for the graph in figure 5.9, because each graph is the result of fewer experimental runs. The error function is a good fit for the data at each Reynolds number as roughly two thirds of the points are within standard deviation of the line. To within the resolution of the method, the shape of the probability versus disturbance amplitude relationship is independent of Reynolds number. Graphs constructed from the data for undeveloped flow, developed flow, the one-jet disturbance generator and the six-jet disturbance generator are found to also have the same shape.

It is possible to understand the error function dependence in the probability versus

a)

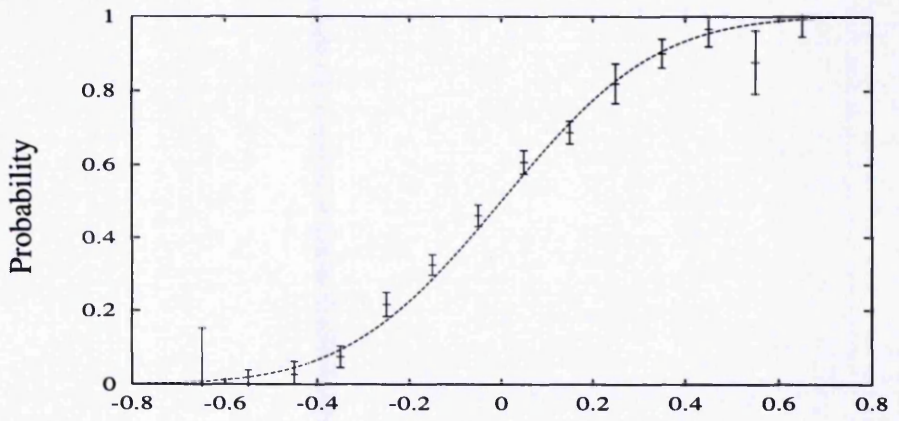

b)

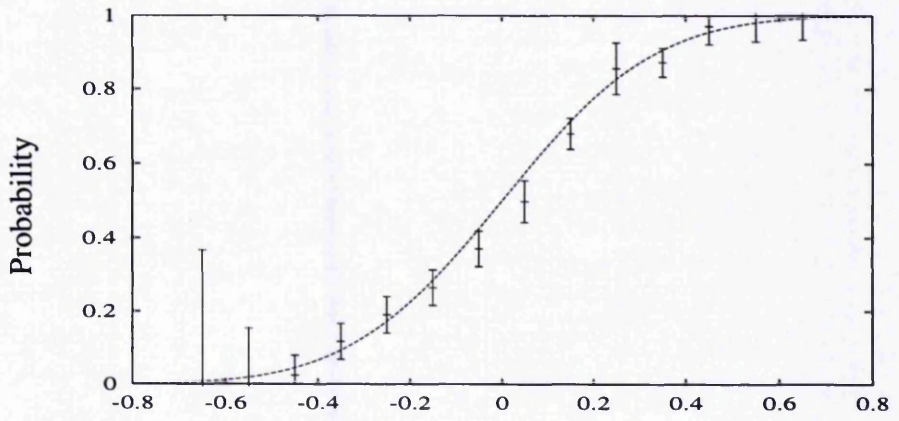

c)

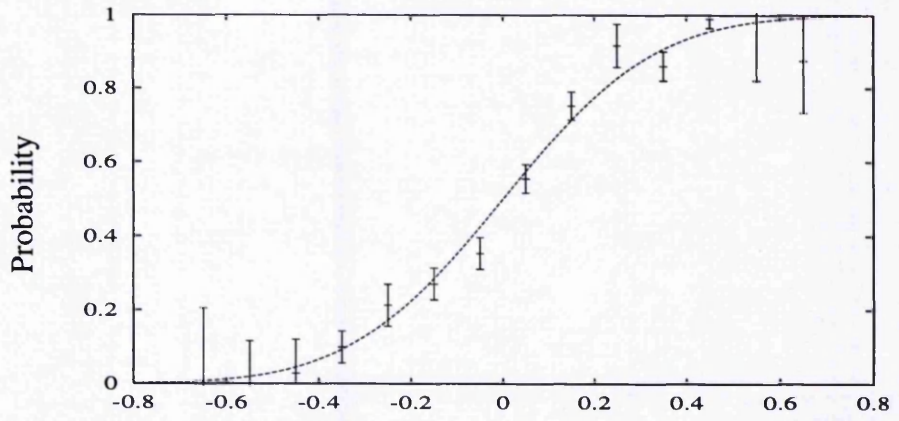

Non-dimensioned Amplitude of Disturbance $((A - A_c)/W)$

FIGURE 5.10. The average shape of the probability curve at Reynolds numbers of a) 2170 b) 3000 c) 4000.

disturbance amplitude relationship by considering the transition to turbulence as a threshold process with superimposed noise. The threshold may then be the value of some global quantity required for transition to be initiated. Examples of such quantities are the total kinetic energy of the perturbation or the total vorticity. Alternatively the threshold may be the amplitude of a single Fourier mode or the derivative of the flow profile at some location. There are likely to be several factors that are important in the transition to turbulence. However the error function dependence of the probability with amplitude implies there is one quantity which is a limiting factor.

The noise itself will consist of external perturbations that effect the main flow as well as small variations in form of perturbation. The size of such noise is very small compared to the size of the perturbation. This was shown by Darbyshire & Mullin (1995) who examined flow velocities close to the disturbance generator. Disturbances that give rise to a stable patch of turbulence and those for which the turbulence decays look the same. It is now suggested how such a threshold process gives rise to an error function dependence of the probability on A.

It is assumed that without noise the amplitude of the threshold quantity, s, would be proportional to the disturbance amplitude so that $s = kA$. Transition would occur when ever $kA > T$, T being the value of the threshold. The presence of Gaussian distributed noise means there is a probability density function, $G(s)$, for the value of s which is

$$G(s) = \frac{1}{\sigma\sqrt{2\pi}} exp\left(\frac{-[s-kA]^2}{2\sigma^2}\right) \tag{5.3}$$

where σ is the standard deviation of s due to the noise. This is a normalised Gaussian with a mean of kA. Transition occurs whenever s exceeds T. Because the distribution is symmetric it is possible to identify T with the quantity kA_c. The probability of transition will be the probability that $s > kA_c$. This is found by integrating G between the threshold and infinity.

$$\begin{aligned} p(A, A_c) &= \int_{kA_c}^{\infty} G(s)ds \\ &= 0.5 + 0.5erf\left(\frac{k[A-A_c]}{\sigma\sqrt{2}}\right) \end{aligned} \tag{5.4}$$

The gradient of this function at $A = A_c$ is $k/2\sigma\sqrt{2}$. Based on a value of e of 2.67 in the fitting function introduced above, the relationship between W and the standard deviation of amplitude of the noise is

$$W = 2 \times 2.67\sigma\sqrt{2}/k \tag{5.5}$$

The value of k is determined by the amount of interaction between the disturbance and the threshold process, σ is the amount of interaction with the noise. When $k > \sigma$ the probabilistic width is small while $k < \sigma$ results in a large value of W.

Chapter 6

Conclusions

This investigation has been concerned with the finite-amplitude stability of pipe flow at the lower range of Reynolds numbers at which turbulent flow is stable. The experiment is performed with fluid drawn though the pipe at constant volume flux, ensuring constant Reynolds number. At these Reynolds numbers the transition to turbulence is probabilistic in nature. The experiment was automated so that large numbers of experimental runs could be performed allowing the probabilities to be calculated accurately. Previous studies of the stability of entrance flow were concerned with the neutral stability curve of developing pipe flow which is believed to exist for Reynolds numbers $\gtrsim$ 7500. The aim of the present study was to extend the knowledge of entrance flow stability to lower Reynolds numbers.

The experimental investigation began by examining the transition to turbulence in fully developed pipe flow. Turbulent puffs were produced when the disturbances were applied with a probability which was dependent on the disturbance amplitude. The way in which the probability changed with amplitude was found to be consistent with the observations of Darbyshire & Mullin (1995). Close examination of the relationship between the probability of transition and the amplitude of disturbance showed that it varied as an error function. The width of the error function depended upon the Reynolds number, the type of disturbance and the size of the critical disturbance amplitude. However,

the probability of transition was always found to vary with the disturbance amplitude as an error function for all of the parameters that were varied.

The differential of an error function is a Gaussian and so the probability density with amplitude function is a Gaussian. One possible cause of this Gaussian behaviour is the interaction of Gaussian noise on the experiment. Another possibility is that the Gaussian statistics originate in the interaction between the disturbance and the fluid flow in the pipe. The size of the effect of the noise is quantified by the probabilistic width. The fact that this is often comparable to the critical disturbance amplitude and is sensitive to changes in the flow parameters suggests that the Gaussian process is important in the transition to turbulence. However, the noise is known to be small compared to the size of the perturbation. Thus it is hard to tell the difference between perturbations that result in sustained transition and those that do not (Darbyshire & Mullin 1995).

The size and speeds of a number of puffs were measured at Reynolds number 2170 in fully developed flow. The speeds of the back and front interfaces were both found to be equal to the mean flow velocity, in agreement with the published literature (Lindgren 1969). This implies that the puffs observed in this experiment are equilibrium puffs. While the speeds of the interfaces of the turbulent puffs in the flow were the same for all puffs, the size of the puffs varied between 3 and 27 pipe diameters. As the speeds of the interfaces were the same, the sizes of the individual puffs remained the same as they were soon after their generation. At higher Reynolds numbers the puffs grow and any difference in their initial size is quickly overwhelmed.

Further comparisons can be made between the results of this and previous investigations from the relationship between the critical amplitude of disturbance and Reynolds number in fully developed flow. The way in which the amplitude of disturbance scales with Reynolds number has been calculated by many researchers. The method used include weakly nonlinear theory (Sen & Maji 1985) and a combination of transient growth and nonlinear effects (Bergstrom 1993, Grossmann 2000, Reddy & Henningson 1993). In all cases the amplitude of disturbance is predicted to vary as a power law as in equa-

tions 1.3 and 1.4. The power of the Reynolds number that the amplitude is proportional to is dependent upon the type of disturbance used or, equivalently, modes that are included for calculation. This is in agreement with the results of Darbyshire & Mullin (1995). Calculating the coefficients in the power law from the experimental data gives values for the scaling factor, Γ, of 0.21 ± 0.06 and 0.51 ± 0.07 (for the one-jet and six-jet disturbance respectively). These compare favourably to those predicted in Sen & Maji (1985) and Grossmann (2000) but are in contrast to the predictions of Bergstrom (1993) and Reddy & Henningson (1993).

The only other experimental investigation of the finite amplitude stability of pipe flow was performed by Darbyshire & Mullin (1995). As in the current investigation it was found that the critical amplitude of disturbance is dependent upon the exact form of the perturbation. However, for all of the perturbations used in both investigations the shape of the relationship between critical disturbance amplitude and Reynolds number was the same. Particularly it was found that the critical disturbance amplitude increased rapidly as the Reynolds number reduced below 2000 for all the perturbations investigated.

The disturbance amplitude required to initiate the transition to turbulence in developing flow was measured as a function of the flow's development. It was found that the developing flow was more stable than the developed flow with respect to both types of disturbance at Reynolds between 2170 and 4000. This trend is in contrast to that of linear stability which predicts that the flow becomes unstable near to the inlet but not in the developed region. As the Reynolds number increases there are some features of the trend in the stability that were found to converge with those of linear stability. However the entrance flow was always found to be more stable with respect to both types of disturbance used.

The finite-amplitude stability curves remain monotonically decreasing functions of the distance from the inlet even at Reynolds number 4000. The monotonic shape of the finite-amplitude stability curve shows no sign of changing as the Reynolds number is increased. This implies that shape of the stability curve changes to the 'J' shape of the

linear neutral stability curve around when the flow first becomes linearly unstable. It is significant that the stability of the flow approaches its fully developed value while at lower stages of flow development at higher Reynolds numbers.

It looks most promising to explain the shapes of the finite-amplitude stability curve at Reynolds numbers of 3000 and 4000 in terms the growing importance of the factors responsible for linear instability. The shape of the $Re = 2170$ curves has little in common with that of neutral stability. The variation in the critical disturbance amplitude with distance from the inlet is different for the two disturbance generators at this Reynolds number, in contrast the curves at $Re = 3000$ and $Re = 4000$. This implies that the mechanism behind the transition to turbulence in the entrance flow is different for the two disturbance generators at $Re = 2170$. The difference in the rates at which the critical disturbance amplitude approaches its fully developed value can be related to the shape of the developing flow profile.

The range of disturbance amplitudes over which the transition process was probabilistic varied depending upon the flow parameters. There was only one correlation that went through the all of the results. For each type of disturbance and at each Reynolds number, the probabilistic width increased when the critical disturbance amplitude increased.

At large Reynolds numbers the entrance flow becomes linearly unstable and so is less stable than the fully developed flow, which is always linearly stable. However, it has been shown that at some Reynolds numbers, for which the entrance flow is linearly stable, it is more stable with respect to the finite-amplitude disturbances used here than the fully developed flow. However, because the form of the perturbation is important in determining the value of the critical disturbance amplitude, it does not follow that the entrance is more stable to all forms of finite perturbation. Further experiments with different types of perturbations would be required to find the generality of this result.

There is a clear difference in the trend of the finite-amplitude stability curve and that of linear stability. It would be interesting to compare the trend in the finite-amplitude sta-

bility of entrance flow with that predicted by transient growth. It may also be instructive to examine the finite-amplitude stability of the flow at higher Reynolds numbers when some parts of the flow are marginally linearly stable. It would be expected that the evolution of the flow would be closer to that predicted by linear stability and therefore easier to analyse and compare with theory.

It is surprising that, as mentioned above, noise has a large effect upon the transition process. The effect of the noise is dependent upon the type of perturbation used. Measuring the probability of transition using different disturbance generators would reveal the conditions under which noise is important. This may illuminate some aspects of the mechanism behind the transition to turbulence in pipe flow.

References

Abbot, A. & Moss, E. (1993), 'The existence of critical reynolds numbers in pipe entrance flows subjected to infinitesimal axisymmetric disturbances', *Physics of Fluids* **6**(10), 3335–3340.

Acheson, D. (1990), *Elementary Fluid Dynamics*, Oxford Applied Mathematics and Computing Series, first edn, Oxford University Press, Walton Street, Oxford OX2 6DP.

Bandyopadhyay, P. (1986), 'Aspects of the equilibrium puff in transitional pipe flow', *J. Fluid Mech* **163**, 439–458.

Bandyopadhyay, P. & Walton, A. (1989), 'Perturbation amplification in the entry region of a transitional pipe flow', *Proc. ICASE/LaRC Stability and Transition Workshop* .

Barlow, R. (1989), *Statistics*, John Wiley & Sons.

Bayly, S., Orszag, S. & Herbert, T. (1988), 'Instability mechanisms in shear-flow transition', *Annu. Rev. Fluid Mech.* **20**, 359–391.

Bergstrom, L. (1993), 'Optimal growth of small disturbances in pipe Poiseuille flow', *Physics of Fluids* **A**(5), 2710.

Boberg, L. & Brosa, U. (1988), 'Onset of turbulence in a pipe', *Z.Naturforschung* **43A**, 697.

Carlson, D. R., Widnall, S. E. & Peters, M. F. (1982), 'A flow-visualization study of transition in plane poiseuille flow', *Journal of Fliud Mechanics* **121**, 487–505.

Darbyshire, A. & Mullin, T. (1995), 'Transition to turbulence in constant-mass-flux pipe flow', *J. Fluid Mech.* **289**, 83–114.

D'Silva, A. & Moss, E. (1994), 'The stability of pipe entrance flows subject to axisymmetric disturbances', *Jornal of Fluids Engineering* **116**, 61–65.

Dauchot, O. & Daviaud, F. (1995), 'Finite amplitude perturbation and spots growth mechanism in plane Couette flow', *Physics of Fluids* **7**(2), 335–343.

Dauchot, O. & Manneville, P. (1997), 'Local versus global concepts in hydrodynamic stability theory', *Journal de Physique II* **7**, 371–389.

Davey, A. & Nguygen, H. (1971), 'Finite-amplitude stability of pipe flow', *J.Fluid Mech.* **45**, 701–720.

Draad, A., Kuiken, G. & Nieuwstadt, F. (1998), 'Laminar-turbulent transition in pipe flow', *J. Fluid Mech* **377**, 267–312.

Drazin, P. & Reid, W. (1981), *Hydrodynamic Stability*, first edn, University of Cambridge Press.

Eckhardt, B. & Mersmann, A. (1999), 'Transition to turbulence in a shear flow', *Physical Review E* **60**(1), 509–517.

Eggels, J., Unger, F., Weiss, M., Westerweel, J., Adrian, R., Friedrich, R. & Nieuwstadt, F. (1994), 'Fully developed pipe flow: acomparision between direct numerical simulation and experiment', *J. Fluid Mech* **268**, 175–209.

Eliahou, S., Tumin, A. & Wygnanski, I. (1998), 'Laminar - turbulent transition in Poiseuille pipe flow subject to periodic perturbation emanating from the wall', *J. Fluid Mech* **8**(361), 333–349.

Fargie, D. & Martin, B. (1971), 'Developing laminar flow in a pipe of circular cross-section', *Proc. Roy Soc. Lond* **321A**, 461–476.

Garg, V. & Gupta, S. (1981), 'Non-parallel effects on the stablity of developing flow in a channel', *Physics of Fluids* **24**(9), 1752–1754.

Grossmann, S. (2000), 'The onset of shear flow turbulence', *Reviews of Modern Physics* **72**(2), 603–618.

Gupta, S. & Garg, V. (1981), 'Effects of velocity distribution on the stablity of developing flow in a pipe', *The Physics of Fluids* **24**, 576–578.

Han, G., Tumin, A. & Wygnanski, I. (2000), 'Laminar-turbulent transition in Poiseuille pipe flow subjected to periodic perturbation emanating from the wall. part 2. late stage of transition', *J. Fluid Mech* **419**, 1–27.

Hornbeck, R. (1963), 'Laminar flow in the entrance region of a pipe', *Applied Scientific Research* **13**(section A), 224–232.

Huang, L. & Chen, T. (1974), 'Stability of the developing pipe flow to subject to non-axisymmetric disturbances', *J. Fluid Mech.* **63**, 183–193.

Joseph, D. & Carmi, S. (1968), 'Stability of Poiseuille flow in pipes, annuli and channels.', *Q. Appl. Math* **26**, 575–591.

Keskel, A. (1961), An experimental study of the stability of pipe flow. II development of the disturbance generator, Technical Report 32-138, Jet Propulsion Laboratory, Califoria Institute of Technology.

Kim, C., Kim, J., Lee, K., Choi, H. & Jhon, M. (2000), 'Mechanical degradation of dilute polymer solutions under turbulent flow', *Polymer* **41**(21), 7611–7615.

Leite, R. (1959), 'An experimental investigation of the stablity of Poiseuille flow', *J. Fluid Mech.* **81**.

Lindgren, E. (1969), 'Propagation velocity of turbulent slugs and streaks in transition pipe flow', *Phys. Fluids* **12**, 418–425.

Mayor, E. & Reskotko, E. (1997), 'Evidence for transient disturbance growth in a 1961 pipe flow experiment', *Physics of Fluids* **9**, 242–244.

Mohanty, A. & Asthana, S. (1978), 'Laminar flow in the entrance region of a smooth pipe', *J. Fluid Mech* **90**(3), 433–447.

Nishioka, M., Iida, S. & Ichikawa, Y. (1975), 'Stability of plane Poiseuille flow', *Journal of Fluid Mechanics* **72**(4), 731–751.

Patera, A. & Orszag, S. (1981), 'Finite-amplitude stability of axisymmetric pipe flow', *J. Fluid Mech.* **112**, 467–474.

Pfenninger, W. (1961), 'Transition in the inlet length of tubes at high reynolds numbers', *Bounbary Layer and Control* pp. 970–980.

Pysik, A. & Heber, J. (1992), 'Experimental realization of Stokes modes of the pipe by Lorentz excitation', *Zeitschrift fur Naturforschung section A-A Journal of Physical Sciences* **47**, 1097–1104.

Reddy, S. & Henningson, D. (1993), 'Energy growth in viscous channel flows', *J. Fluid Mech* **252**, 209–238.

Reynolds, O. (1883), 'An experimental investigation of the circumstances which determine whether the motion of water shall be direct or sinuous and the law of resistance in parallel channels.', *Proceedings of the Royal Society London* **35**, 84–99.

Romanov, V. (1973), 'Stability of plane-Couette flow', *Functional Analytical Applied Mathematics* **7**, 137.

Salwen, H. & Grosch, C. (1972), 'The stability of Poiseuille flow in a pipe of circular cross-section', *J.Fluid Mech.* **54**, 93–112.

Sarpkaya, T. (1975), 'A note on the stability of developing laminar pipe flow subject to axisymmetric and non-axisymmetric disturbances', *J. Fluid Mech* **68**, 345–351.

Schlichting (1960), *Boundary-layer Theory*, McGraw-Hill series in Mechanical Engineering, third edn, McGraw-Hill.

Schmid, P. J.and Henningson, D. (1994), 'Optimal energy density growth in Hagen-Poiseuille flow', *J.Fluid Mech* **277**, 197–225.

Sen, P.K. Venkateswarlu, D. & Maji, S. (1985), 'On the stability of pipe-Poiseuille flow to finite-amplitude axisymmetric and non-axisymmetric disturbances', *J. Fluid Mech* **158**, 289–316.

Shan, H., Ma, B., Zhang, Z. & Nieuwstadt, F. (1998), 'Direct numerical simulation of transition in pipe flow under the influence of wall disturbances', *International Journal of Heat and Fluid Flow* **19**, 320–325.

Sparrow, E., Lin, S. & Lundgren, T. (1964), 'Flow development in the hydrodynamic entrance region of tubes and ducts', *The Physics of Fluids* **7**, 338–342.

Tatsumi, T. (1952), 'Stablity of laminar inlet flow prior to the formation of Poiseuille regime', *Phys. Soc. Japan* **7**, 489–501.

Trefethen, L., Trefethen, A., Reddy, S. & Discoll, T. (1993), 'Hydrodynamic stablility without Eigenvalues', *Science* **261**, 578.

Tritton, D. (1988), *Physical Fluid Dynamics*, second edn, Oxford University Press.

Weast, R., ed. (1980), *Hand Book of Physics and Chemistry*, 61 edn, CRC Press Inc.

Wygnanski & Champagne (1973), 'On transition in a pipe flow 1.', *J. Fluid Mech.* **59**, 281–335.

Wygnanski, I. S. M. & Friedman, D. (1975), 'On transition in a pipe flow 2. the equilibrium puff', *J.Fluid Mech.* **69**, 283–304.

Zikanov, O. (1996), 'On the instability of pipe poiseuille flow', *Physics of Fluids* **8**(11), 1–10.